Loss of collectivity in the transitional ^{156}Er nucleus at high spin

E. S. Paul,[1] S. V. Rigby,[1] M. A. Riley,[2] J. Simpson,[3] D. E. Appelbe,[3] D. B. Campbell,[2] P. T. W. Choy,[1] R. M. Clark,[4] M. Cromaz,[4] A. O. Evans,[1] P. Fallon,[4] A. Görgen,[4,*] D. T. Joss,[3,†] I. Y. Lee,[4] A. O. Macchiavelli,[4] P. J. Nolan,[1] A. Pipidis,[2] D. Ward,[4] and I. Ragnarsson[5]

[1]*Oliver Lodge Laboratory, University of Liverpool, Liverpool L69 7ZE, United Kingdom*
[2]*Department of Physics, Florida State University, Tallahassee, Florida 32306, USA*
[3]*STFC Daresbury Laboratory, Daresbury, Warrington WA4 4AD, United Kingdom*
[4]*Nuclear Science Division, Lawrence Berkeley National Laboratory, Berkeley, California 94720, USA*
[5]*Division of Mathematical Physics, LTH, Lund University, Post Office Box 118, S-22100 Lund, Sweden*

(Received 5 February 2009; published 29 April 2009)

The ^{114}Cd(^{48}Ca, $6n\gamma$) reaction at 215 MeV has been investigated using the Gammasphere spectrometer to study the high-spin structure of the nucleus $^{156}_{68}$Er$_{88}$. Many new transitions have been established along with definitive spin-parity level assignments from a high-fold angular-distribution analysis. In addition, absolute $B(M1)$ and $B(E1)$ strengths have been inferred from measured γ-ray branching ratios. Strong $B(E1)$ strength (10^{-3} W.u.) is discussed in terms of possible octupole collectivity at low spin. At high spin, this nucleus undergoes a Coriolis-induced shape transition from a prolate state of collective rotation to a noncollective, triaxial-oblate configuration. The yrast positive-parity structure ultimately terminates in an energetically favored oblate state at $I^{\pi} = 42^{+}$. Several weak high-energy γ-ray transitions have been discovered that feed this favored state. State-of-the-art cranked Nilsson-Strutinsky calculations are used to interpret the high-spin behavior of ^{156}Er and comparisons are made with other $N = 88$ isotones.

DOI: 10.1103/PhysRevC.79.044324 PACS number(s): 27.70.+q, 21.10.Re, 23.20.Lv, 23.20.En

I. INTRODUCTION

The generation of angular momentum (spin, I) in the atomic nucleus, a finite mesoscopic system, has always been at the forefront of nuclear-structure physics, from both experimental and theoretical viewpoints. A deformed prolate nucleus can increase its spin by *collective* rotation about an axis perpendicular to its symmetry axis, leading to discrete energy levels that approximate quantum-rotor behavior [i.e., $E(I) \propto I(I+1)$] and consequently the observation of regular rotational bands in γ-ray emission spectra. As the angular momentum is increased, however, nuclei exhibit dramatic Coriolis-induced *alignments* (i.e., breaking of nucleonic pairs by the fictive force in a rotating frame of reference). As more and more valence nucleons align with the axis of rotation, a larger fraction of the nuclear spin is generated by single-particle *noncollective* contributions. Eventually, the angular momentum is wholly generated by the single-particle contributions of a finite number of *valence* nucleons in equatorial orbits outside a closed spherical (doubly magic) core, which can give certain nuclei an *oblate* appearance. This change of spin generation from collective to noncollective "rotation about the symmetry axis" [1,2] manifests itself experimentally as *band termination* [3,4] in γ-ray spectra when regular rotational sequences appear to end. Such high-spin, valence-space terminating bands in heavy nuclei were first identified and interpreted in nuclei around $^{156}_{68}$Er$_{88}$ [3,5–10] at angular momentum values of $40\hbar$–$50\hbar$; a comprehensive summary of terminating bands is given in Ref. [11].

Although clear examples of the special terminating states had been identified in a number of erbium isotopes [7,12–14], until the present work [15,16] almost nothing was known about the higher spin states lying above band-termination states in isotopes close to the textbook example of ^{158}Er [17,18]. Higher spin can only be generated by energetically expensive *core-excited* configurations involving particle-hole excitations of the spherical nuclear core. The present experiment was undertaken to identify and delineate the nuclear excitation spectrum of these core-breaking states and allow comparisons to theoretical predictions. To this end, many weakly populated (at the 10^{-4}–10^{-3} level) states lying 1–2.5 MeV above the terminating states in odd-N ^{157}Er were established from the current experiment [15,16], while similar features were seen, to a lesser extent, in the neighboring ^{156,158}Er even-even isotopes [19,20]; the present paper details the results for ^{156}Er. The level scheme of ^{156}Er has been extended with many new transitions along with definitive spin-parity level assignments from a high-fold angular-distribution analysis. In addition, $B(M1)/B(E2)$ and $B(E1)/B(E2)$ ratios of reduced transition probabilities have been extracted from measured γ-ray branching ratios, from which absolute $B(M1)$ and $B(E1)$ strengths have been deduced in this nucleus.

The yrast band of ^{156}Er shows a sudden collective-noncollective phase change at $I \approx 30$ [7,10,21] and terminates in an energetically favored oblate state at 14.4 MeV with $I^{\pi} = 42^{+}$. This state represents a valence-space termination where the 10 particles outside the ^{146}Gd closed core generate the total nuclear angular momentum in a noncollective oblate configuration. Five transitions, four of them newly identified, have been established in this work that directly feed this

[*]Present address: DAPNIA/SPhN CEA-Saclay, Bat 703 l'Orme des Merisiers, F-91191 Gif-sur-Yvette, France.

[†]Present address: Oliver Lodge Laboratory, University of Liverpool, Liverpool L69 7ZE, United Kingdom.

 ©2009 The American Physical Society

favored terminating state. Furthermore, the four new feeding transitions have been assigned $\Delta I = 2$ (quadrupole) character from the present analysis; in contrast, the fifth feeding transition has been assigned $\Delta I = 1$ character (dipole), in agreement with previous work [7]. State-of-the-art cranked Nilsson-Strutinsky calculations are used to interpret the high-spin behavior of ^{156}Er. Higher spin, beyond $42\hbar$, is generated by invoking proton particle-hole excitations across the $Z = 64$ shell gap, in effect increasing the number of valence nucleons (particles *and* holes) that can contribute to the nuclear angular momentum. Comparisons with other $N = 88$ isotones ($Z = 64$ to 70), which have been observed to high spin, are also discussed.

II. EXPERIMENTAL DETAILS AND RESULTS

The high-spin structure of ^{156}Er was studied at the 88 Inch Cyclotron of the Lawrence Berkeley National Laboratory, using the Gammasphere γ-ray spectrometer [22] containing 102 HPGe detectors. A ^{48}Ca beam of energy 215 MeV was used to bombard two stacked thin self-supporting foils of ^{114}Cd, of total thickness 1.1 mg/cm^2, producing ^{156}Er through the ^{114}Cd(^{48}Ca, $6n\gamma$) reaction. A total of 1.2×10^9 events were recorded to tape when at least seven Compton-suppressed HPGe detectors fired in prompt time coincidence.

In the offline analysis, approximately 6.5×10^{10} quadruple (γ^4) coincident events were unfolded from the data and replayed into a RadWare-format four-dimensional hypercube [23,24], with a nonlinear gain compression, for subsequent analysis. The dominant nuclei observed correspond to pure neutron evaporation; the nuclei ^{156}Er ($6n$), ^{157}Er ($5n$), and ^{158}Er ($4n$) were measured to be populated in the ratio 0.4:1.0:1.0, approximately, in the hypercube. Hence conditions were not optimal in this experiment for the study of ^{156}Er. Nevertheless, the high-fold nature of the present data set allowed a thorough investigation of this nucleus to be performed.

One-dimensional spectra, multiply gated by transitions in ^{156}Er, were also unfolded directly from the data up to fold eight (γ^8), using the technique of Ref. [25]. Such an analysis proved pivotal in extracting high-quality spectra of extremely weak high-spin bands in ^{157,158}Er [26] from this data set. This analysis technique has been extended to produce spectra corresponding to the detectors in the rings of Gammasphere at a fixed angle θ to the beam direction, from which it is possible to perform an angular-distribution analysis of transitions. The intensities of γ-ray transitions assigned to ^{156}Er, measured at a specific angle θ, were fitted to the angular-distribution function,

$$W(\theta) = 1 + A_2 P_2(\cos\theta) + A_4 P_4(\cos\theta), \qquad (1)$$

to extract A_2 and A_4 coefficients. For some transitions with unphysically large A_4 coefficients, A_4 was set to zero and only an A_2 coefficient extracted. Stretched quadrupole transitions are characterized by positive A_2 values and pure stretched dipole transitions by negative A_2 values. This analysis provides only multipole order of the transitions in ^{156}Er; relative parity assignments are adopted from previous work [7]. Figures 1 and 2 show examples of such γ^4-gated fits for strong low-spin and

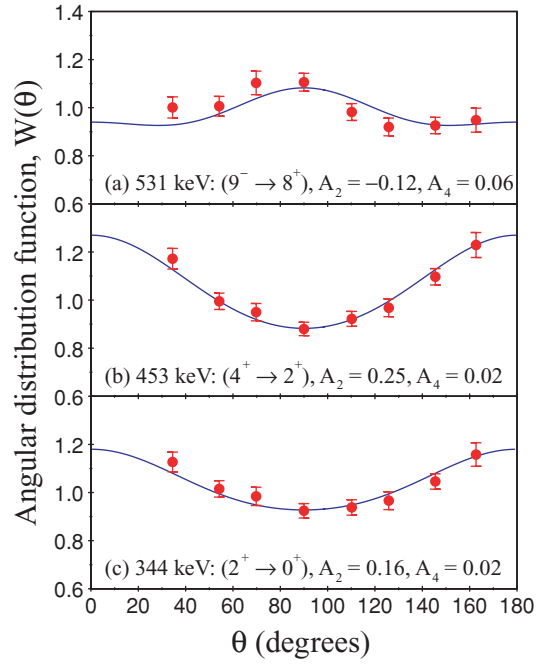

FIG. 1. (Color online) Examples of γ^4-gated angular distributions for some of the strong, low-spin transitions in ^{156}Er. The curves (blue) are fits of the angular-distribution function, $W(\theta)$, to the experimental data (red).

weaker high-spin transitions in ^{156}Er, respectively. The gating transitions consisted of all the $E2$ transitions of the positive-parity bands 1–3 of ^{156}Er, as shown in Fig. 3, except those transitions that are also strong transitions in the contaminant ^{157,158}Er isotopes.

The level scheme deduced for ^{156}Er is displayed in Fig. 3, based on high-fold γ-ray coincidence relationships in addition to relative-intensity arguments. The band structures have been labeled bands 1–6 to facilitate the discussion. The measured γ-ray transition energies, relative intensities, and angular-distribution coefficients are listed in Table I, together with deduced spin-parity assignments; examples of coincident γ-ray spectra are shown in Figs. 4 and 5. Five transitions, of energies 163, 191, 243, 266, and 282 keV, are listed in Table I, including angular-distribution information, but could not be placed in the level scheme of Fig. 3. The nature of the present high-fold analysis does suggest that these transitions belong to ^{156}Er, although two of these transitions have energies (191 and 266 keV) very similar to the strongest ($E2$) transitions in ^{158}Er and ^{157}Er, respectively. Moreover, these five unplaced transitions all appear to be in coincidence with both the ground-state band of ^{156}Er (band 1) and the yrast negative-parity band 4a.

The present results confirm and strengthen the previous work on ^{156}Er [7] through the observation of many intraband transitions. The observation of these weakly populated transitions was only possible through the high-fold analysis afforded by the present data, especially with strong contamination from ^{157}Er ($5n$) and ^{158}Er ($4n$). Furthermore, the high-fold analysis was crucial in the placement of multiplets with very similar

TABLE I. Energies, intensities, angular-distribution coefficients, and spin-parity assignments for the transitions assigned to ^{156}Er. The numbers in the final column correspond to the labeling of the bands in Fig. 3.

E_γ (keV)[a]	I_γ[b]	A_2	A_4	Multipolarity	Assignment	Band
118.3		−0.3(2)	≡0.0	$E1$	$13^- \rightarrow 12^+$	4a → 1
163[c]		−0.1(1)	≡0.0	(dipole)		
176.1					$21^- \rightarrow 21^-$	6a → 4b
186.0					$23^- \rightarrow 23^-$	6a → 4b
191[c]		−0.08(4)	≡0.0	(dipole)		
202.5					$21^- \rightarrow 20^-$	4b → 5a
218.3	2.2	−0.21(3)	0.03(4)	$M1/E2$	$36^+ \rightarrow 35^+$	1 →
234.6					$25^- \rightarrow 24^-$	6a → 5b
243[c]		−0.6(1)	0.0(1)	$(M1/E2)$		
266[c]		0.20(5)	−0.06(6)	$(E2)$		
270.4	2.9	0.3(1)	0.0(1)	$E1, \Delta I = 0$	$10^- \rightarrow 10^+$	5a → 1
282[c]		0.16(8)	0.05(11)	$(E2)$		
283.4					$36^- \rightarrow (35^-)$	5b →
289.8					$13^- \rightarrow 12^-$	6 → 5a
290.4	18	−0.10(3)	0.03(4)	$E1$	$11^- \rightarrow 10^+$	4a → 1
292.4					$27^- \rightarrow 26^-$	6a → 5b
301.8	5.2	0.15(6)	−0.08(8)	$E2$	$10^+ \rightarrow 8^+$	5a → 5
306.7					$22^+ \rightarrow 21^-$	2 → 4a
344.3	≡100	0.16(3)	0.02(4)	$E2$	$2^+ \rightarrow 0^+$	1
345						2a
356.3					$15^- \rightarrow 14^-$	6 → 5a
359.5		−0.05(8)	≡0.0	$E1$	$30^+ \rightarrow 29^-$	3 → 6a
369.8					$23^- \rightarrow 22^-$	4a → 5b
376.6					$19^- \rightarrow 18^-$	4b → 5a
378.5					$21^- \rightarrow 20^-$	6a → 5a
384.5					$22^- \rightarrow 21^-$	5b → 4a
387.4					$42^+ \rightarrow 40^+$	3 → 3a
390.0		0.46(5)	−0.02(6)	$E2$	$6^- \rightarrow 4^-$	5
396.7	2.1				$8^- \rightarrow 6^-$	5
397.5	1.1				$14^+ \rightarrow 12^+$	1a → 1
407.8					$17^- \rightarrow 16^-$	6 → 5a
413.7	7.0				$10^- \rightarrow 9^-$	5a → 4a
417.3	2.0				$7^- \rightarrow 5^-$	4
421.5					$29^- \rightarrow 28^-$	6a → 5b
433.6	31	0.29(3)	0.01(4)	$E2$	$11^- \rightarrow 9^-$	4a
435.1					$20^+ \rightarrow 19^-$	2 → 4a
447.9	2.2				$11^- \rightarrow 10^+$	6 → 1
452.6	82	0.25(3)	0.02(4)	$E2$	$4^+ \rightarrow 2^+$	1
460.8	7.2	0.5(1)	0.0(1)	$E2$	$9^- \rightarrow 7^-$	4a → 4
460.9	1.6				$12^- \rightarrow 11^-$	5a → 4a
479.6					$22^- \rightarrow 21^-$	5b → 4b
480.9	9.7	0.38(6)	≡0.0	$E2$	$12^- \rightarrow 10^-$	5a
487.1					$\rightarrow 24^+$	2a →
488.8					$31^- \rightarrow 30^-$	6a → 5b
490.8					$19^- \rightarrow 18^-$	6 → 5a
507					$\rightarrow 43^{(-)}$	
508.4	42	0.31(3)	≡0.0	$E2$	$13^- \rightarrow 11^-$	4a
522.0					$14^- \rightarrow 13^-$	5a → 4a
522.2	15	0.43(3)	0.01(4)	$E2$	$14^+ \rightarrow 12^+$	1
530.6	31	−0.12(3)	0.06(4)	$E1$	$9^- \rightarrow 8^+$	4a → 1
536.1					$\rightarrow 24^+$	2a → 2
539.2					$25^- \rightarrow 23^-$	6a → 4a
543.6	69	0.36(3)	−0.02(4)	$E2$	$6^+ \rightarrow 4^+$	1
543.8	14			$E2$	$16^+ \rightarrow 14^+$	1a
547.2					$24^- \rightarrow 23^-$	5b → 4b
557.3					$16^- \rightarrow 15^-$	5a → 4a

TABLE I. (*Continued.*)

E_γ (keV)[a]	I_γ[b]	A_2	A_4	Multipolarity	Assignment	Band
554.4	2.1	0.46(3)[c]	≡0.0[c]	$E2$	$42^+ \rightarrow 40^+$	3
556.0	8.6	0.46(3)[c]	≡0.0[c]	$E2$	$18^+ \rightarrow 16^+$	2
562.9					$20^- \rightarrow 19^-$	5a → 4a
569.8	12	0.36(6)	≡0.0	$E2$	$14^- \rightarrow 12^-$	5a
572.0					$8^- \rightarrow 7^-$	5 → 4
577.5						2a
579.8	1.1				$30^+ \rightarrow 28^+$	3 → 2
585.9					$18^- \rightarrow 17^-$	5a → 4a
587.1					$21^- \rightarrow 19^-$	4b
589.9					$26^+ \rightarrow 24^+$	1a →
591.6	2.8[d]				$11^- \rightarrow 9^-$	6 → 4a
591.6	2.8[d]				$13^- \rightarrow 11^-$	6
592.1					$6^- \rightarrow 5^-$	5 → 4
593.0	8.4				$20^+ \rightarrow 18^+$	2
595.8	5.0				$25^- \rightarrow 23^-$	6a
602.5	39	0.3(1)	≡0.0	$E2$	$15^- \rightarrow 13^-$	4a
605.9	2.7				$23^- \rightarrow 21^-$	4b
611					$\rightarrow 44^+$	
617.4	5.2				$23^- \rightarrow 21^-$	6a
617.5	53	0.37(3)	0.00(4)	$E2$	$8^+ \rightarrow 6^+$	1
626.3	14	0.41(3)	−0.03(4)	$E2$	$18^+ \rightarrow 16^+$	1a
626.9	1.7				$18^+ \rightarrow 17^-$	2 → 4a
632.0					$40^+ \rightarrow 38^+$	3a
635.1					$38^- \rightarrow 36^-$	5b
636.2	3.3				$15^- \rightarrow 13^-$	6
637.4					$28^+ \rightarrow 26^+$	3 → 2
639.4	8.9	0.35(6)	≡0.0	$E2$	$16^- \rightarrow 14^-$	5a
641.7					$8^- \rightarrow 8^+$	5 → 1
649.8	3.5				$21^- \rightarrow 19^-$	6a → 6
651.1					$34^- \rightarrow 33^-$	→ 6a
664.4	3.4	0.40(3)	0.03(4)	$E2$	$40^+ \rightarrow 38^+$	1
674.1	47	0.36(3)	−0.01(4)	$E2$	$10^+ \rightarrow 8^+$	1
673.6					$19^- \rightarrow 17^-$	4b → 6
673.9	6.1				$24^- \rightarrow 22^-$	5b
676.4	22				$17^- \rightarrow 15^-$	4a
681.6					$21^- \rightarrow 19^-$	4a → 4b
681.8	20	0.43(3)	−0.02(4)	$E2$	$12^+ \rightarrow 10^+$	1
682.4	3.3				$34^+ \rightarrow 32^+$	3
682.9	3.0				$22^- \rightarrow 20^-$	5b → 5a
683.0					$30^+ \rightarrow 28^+$	3 → 1a
686.8	5.9				$26^- \rightarrow 24^-$	5b
688.6	12				$7^- \rightarrow 6^+$	4 → 1
688.5	1.7				$27^- \rightarrow 25^-$	4b
691.0	2.7				$17^- \rightarrow 15^-$	6
702.2					$36^+ \rightarrow 34^+$	3 →
703.7	6.8				$18^- \rightarrow 16^-$	5a
710.2	13	0.17(3)	−0.09(5)	$E2$	$20^+ \rightarrow 18^+$	1a
720.1	3.2	0.12(3)	0.04(4)	$M1/E2$	$35^+ \rightarrow 34^+$	→3
731.7	8.8	0.36(4)	≡0.0	$E2$	$22^+ \rightarrow 20^+$	2
733.3	2.4				$25^- \rightarrow 23^-$	4b
744.2	7.8[d]	0.33(4)[d]	0.01(5)[d]	$E2$	$33^- \rightarrow 31^-$	6a
744.2	7.8[d]	0.33(4)[d]	0.01(5)[d]	$E2$	$27^- \rightarrow 25^-$	6a
745.7					$30^+ \rightarrow$	3 → 2a
747.0	5.0				$16^+ \rightarrow 15^-$	2 → 4a
752.0					$23^- \rightarrow 21^-$	4a
760.8	4.2				$20^- \rightarrow 18^-$	5a
765.5	2.1				$21^- \rightarrow 19^-$	4b → 4a

TABLE I. (*Continued.*)

E_γ (keV)[a]	I_γ[b]	A_2	A_4	Multipolarity	Assignment	Band
766.0	3.0				$28^- \rightarrow 26^-$	5b
766.5	5.0				$26^+ \rightarrow 24^+$	2
766.7	4.5	0.40(3)	−0.03(4)	$E2$	$26^+ \rightarrow 24^+$	1a
766.7	2.8				$28^+ \rightarrow 26^+$	3 → 1a
766.7	3.4				$32^+ \rightarrow 30^+$	3
772.9	8.9	0.43(3)	−0.05(4)	$E2$	$22^+ \rightarrow 20^+$	1a
780.9	5.8				$24^+ \rightarrow 22^+$	2
783.9	16				$19^- \rightarrow 17^-$	4a
787.5	3.3				$19^- \rightarrow 17^-$	6
793.0	1.1				$27^- \rightarrow 25^-$	6a → 4b
793.0					$23^- \rightarrow 21^-$	6a → 4a
798.9	2.2	0.49(4)	≡0.0	$E2$	$30^+ \rightarrow 28^+$	3
806.8	1.4				$12^+ \rightarrow 10^+$	1
813.5					$5^- \rightarrow 4^+$	4 → 1
826.4	4.4				$30^- \rightarrow 28^-$	5b
826.9	5.6	0.48(3)	≡0.0	$E2$	$24^+ \rightarrow 22^+$	1a
831.9					$40^+ \rightarrow 38^+$	3a → 3
838.8	2.1				$32^- \rightarrow 30^-$	5b
845.7					$36^- \rightarrow 34^-$	5b →
857.4	2.2				$28^+ \rightarrow 26^+$	2
859.7	3.3				$21^- \rightarrow 19^-$	4a
863.5	2.2				$6^- \rightarrow 6^+$	5 → 1
882.9	3.3	0.39(3)	≡0.0	$E2$	$28^+ \rightarrow 26^+$	1a
894.0	7.2[d]				$31^- \rightarrow 29^-$	6a
894.0	7.2[d]				$29^- \rightarrow 27^-$	6a
908.4					$29^- \rightarrow 27^-$	4b
908.4					$31^- \rightarrow 29^-$	4b
918.4					$34^+ \rightarrow 32^+$	→ 3
920.9					$34^- \rightarrow 32^-$	5b
924.8					$20^+ \rightarrow 18^+$	2 → 1a
938.4	3.4	0.40(4)	0.06(5)	$E2$	$36^+ \rightarrow 34^+$	3
946.4					$16^+ \rightarrow 14^+$	2 → 1a
957.9					$18^+ \rightarrow 16^+$	2 → 1a
964.0	1.1				$19^- \rightarrow 17^-$	4b → 4a
965.3					$17^- \rightarrow 15^-$	6 → 4a
969.8					$36^- \rightarrow 34^-$	5b
1003.1	1.1				$24^+ \rightarrow 22^+$	→ 1a
1016.4					$4^- \rightarrow 4^+$	5 → 1
1045.5					$34^- \rightarrow 32^-$	→ 5b
1048.1					$(35^-) \rightarrow 33^-$	6a
1057.1		−0.34(5)	0.09(7)	($E1$)	$43^{(-)} \rightarrow 42^+$	→ 3
1076.2					$19^- \rightarrow 17^-$	6 → 4a
1081.0					$33^- \rightarrow 31^-$	4b
1167.1	3.3	0.38(3)	−0.02(4)	$E2$	$38^+ \rightarrow 36^+$	3
1212.9					$(35^-) \rightarrow 33^-$	→ 6a
1342		0.21(6)	0.07(8)	$E2$	$44^+ \rightarrow 42^+$	→ 3
1367.0		0.28(9)	0.03(11)	$E2$	$38^+ \rightarrow 36^+$	3a → 3
1392		0.5(2)	≡0.0	$E2$	$44^+ \rightarrow 42^+$	→ 3
1621		0.3(1)	≡0.0	$E2$	$44^+ \rightarrow 42^+$	→ 3
2161		0.4(1)	≡0.0	$E2$	$44^+ \rightarrow 42^+$	→ 3

[a]The γ-ray energies are estimated to be accurate to ±0.3 keV for the strong transitions ($I_\gamma > 10$), rising to ±0.6 keV for the weaker transitions.

[b]Intensities not listed are less than 1% of the 344-keV ($2^+ \rightarrow 0^+$) transition. Errors on the intensities are estimated to be less than 5% of the quoted values for strong transitions ($I_\gamma > 10$) and less than 10% for the weaker transitions.

[c]Transition not placed in the level scheme shown in Fig. 3.

[d]Doublet: Value given for composite peak.

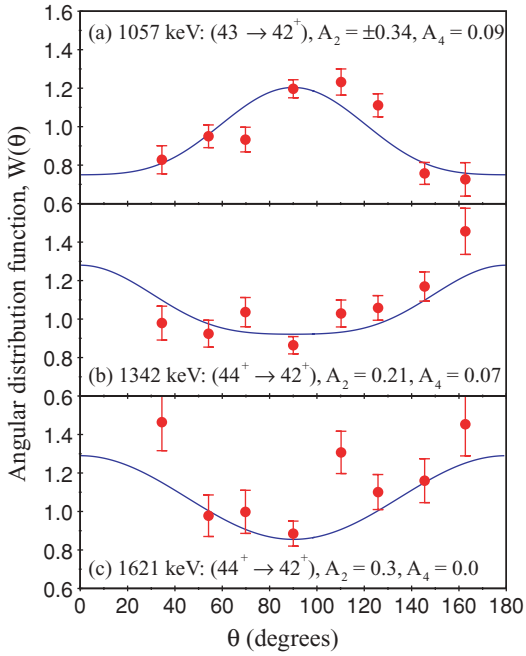

FIG. 2. (Color online) The γ^4-gated angular distributions for three of the weak transitions feeding the favored 42^+ state. The curves (blue) are fits of the angular-distribution function, $W(\theta)$, to the experimental data (red).

energies in the ^{156}Er level scheme (e.g., transitions of energies ≈682 and ≈766 keV; see Table I).

A. Positive-parity structures: bands 1–3

States of positive parity were previously established in ^{156}Er up to $I^\pi = 42^+$ [7] and are corroborated by the present analysis. Band 1 in Fig. 3 represents the ground-state rotational band in ^{156}Er. Above $I^\pi = 10^+$, band 1a becomes yrast and another positive-parity structure, namely band 2, is observed parallel to band 1a. In addition to decaying to band 1a, band 2 also decays into negative-parity band 4a. At $I^\pi = 28^+$, band 3 becomes yrast and extends up to $I^\pi = 42^+$ through an irregular set of levels. Band 3 directly feeds bands 1a and 2 but also decays through an intermediate structure, namely band 2a, into band 2. Band 3 also decays into negative-parity band 6a through a 359-keV transition.

The terminating 42^+ state of band 3 decays into a second 40^+ state (band 3a) through a 387-keV transition; this 40^+ state then decays back into the 38^+ state of band 3 via an 832-keV transition. Nonyrast band 3a only continues down to a 38^+ state before decaying into band 3 through the 1367-keV $E2$ transition. The present ordering of the 1367- to 632-keV transitions is reversed with respect to previous experimental work [7] but is consistent with previous theoretical work [8], based on measured γ-ray intensities; the 1167-keV transition depopulating the yrast 38^+ state of band 3 is about an order of magnitude more intense than the 1367-keV transition depopulating the nonyrast 38^+ state of band 3a. Two other levels, with $I^\pi = 34^+$ and 35^+, are connected to bands 3, consistent with previous work [7].

TABLE II. Feeding intensities of the 42^+ state of band 3 normalized to the 554-keV ($42^+ \rightarrow 40^+$) transition, which carries 2.2% of the intensity of the 344-keV ($2^+ \rightarrow 0^+$) transition.

E_γ (keV)	$I_i^\pi \rightarrow I_f^\pi$	Relative intensity (%)
554	$42^+ \rightarrow 40^+$	≡100
1057	$43 \rightarrow 42^+$	13.8(4)
1342	$44^+ \rightarrow 42^+$	7.0(3)
1392	$44^+ \rightarrow 42^+$	1.7(3)
1621	$44^+ \rightarrow 42^+$	4.8(3)
2161	$44^+ \rightarrow 42^+$	1.4(3)
		$\sum = 28.7(7)$

Five high-energy transitions (1057, 1342, 1392, 1621, and 2161 keV) directly feed the 42^+ state of band 3, as labeled in the high-fold γ-ray coincidence spectra shown in Fig. 4. Apart from the 1057-keV transition, these transitions are newly identified in the present work. The placement of these transitions is corroborated by the γ^4 hypercube analysis. However, other possible weak transitions beyond $E_\gamma = 1.5$ MeV are evident in Fig. 4 and may represent other feeding transitions of the 42^+ state. The angular-distribution analysis confirms the dipole nature of the known 1057-keV transition [7] and implies stretched-quadrupole ($E2$) character for the other four transitions; Fig. 2 shows the results for the 1057-, 1342-, and 1621-keV transitions.

The measured intensities of the transitions feeding the $I^\pi = 42^+$ terminating state of band 3 are given in Table II, relative to the intensity of the 554-keV transition that depopulates this state. The 554-keV transition carries only 2.2% of the intensity of the 344-keV $2^+ \rightarrow 0^+$ transition of ^{156}Er. The intensities listed in Table II were obtained from a triple-gated coincidence spectrum using a combination of the transitions of band 3 below $I^\pi = 40^+$ as the gates. A total feeding intensity for the 42^+ state of 29% is found, similar to the feeding intensities of the band-terminating states in neighboring ^{157}Er [15,16].

From the high-fold coincidence analysis, a transition of energy 611 keV is placed above the yrast 44^+ state at 15763 keV that feeds the terminating 42^+ state of band 3 through the 1342-keV transition. Similarly, a transition of energy 507 keV is placed above the 1057-keV dipole transition that depopulates the state at 15478 keV. The multipolarities of the 507- and 611-keV transitions could not be determined.

B. Negative-parity structures: bands 4–6

Triple-gated γ-ray coincidence spectra associated with bands 4–6, obtained from the hypercube, are shown in Fig. 5. The lower portion of the odd-spin band 4a is yrast and was originally established using only a pair of Ge(Li) detectors [27]. This band was subsequently extended up to $I^\pi = 31^-$ (band 4b) and down to $I^\pi = 7^-$ (band 4) using an array of 21 Compton-suppressed HPGe detectors [7]. The present work has added a γ ray of energy 1081 keV to the top of the band ($33^- \rightarrow 31^-$) and a weak γ ray of energy 417 keV to the bottom of the band ($7^- \rightarrow 5^-$). This latter transition connects to a previously known $I^\pi = 5^-$ state, observed in the β^+

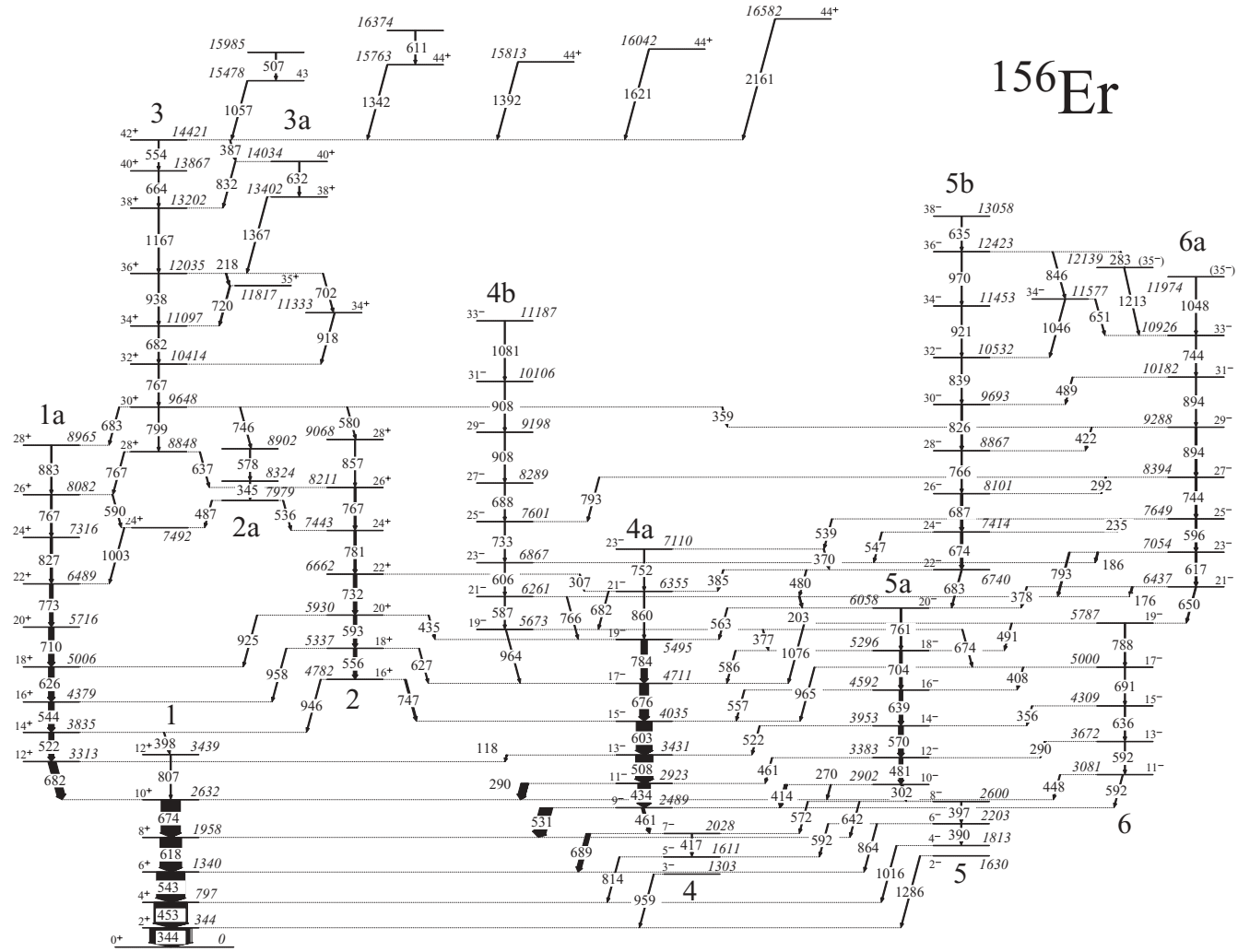

FIG. 3. Level scheme deduced for ^{156}Er from the present work. Energies are labeled in keV and the widths of the arrows are proportional to the transition intensities. The properties of the transitions are listed in Table I.

and electron-capture radioactive decay of ^{156}Tm [28], which decays to the ground-state band (band 1) via a transition of energy 814 keV. The known 3^- state [28], which decays to the ground-state band through a 959-keV transition, is also drawn in Fig. 3 and is assumed to be the continuation of band 4; the in-band $5^- \rightarrow 3^-$ transition was not, however, observed in the present data.

The even-spin band 5 was previously observed from $I^\pi = 6^-$ up to 38^- [7]. The present data has identified a weak transition of energy 390 keV that decays from the 6^- state into a previously known 4^- state [28], which in turn decays into the ground-state band (band 1) through a transition of energy 1016 keV. A lower lying, known 2^- state [28] is also drawn in Fig. 3.

The odd-spin band 6 was previously observed up to $I^\pi = 33^-$ and also linked to higher spin states of band 5b via an intermediate 34^- state at an energy of 11577 keV [7]. The present data extends the band to higher spin (35^-) with the placement of two parallel transitions, of energies 1048 and 1213 keV, above the $I^\pi = 33^-$ level. A transition of energy 283 keV links the 36^- state of band 5b to the (35^-) level at 12139 keV, which subsequently decays into the 33^- level of band 6a through the 1213-keV transition. The placement of the 744- and 894-keV doublets within band 6a is confirmed through the observation of weak intraband dipole transitions (235, 292, 422, and 489 keV) linking band 6a to band 5b. Similarly, at lower spin, many new intraband dipole transitions have been identified linking band 6 to band 5a and also band 5a to band 4a.

III. DISCUSSION

The ^{156}Er nuclide, with only 10 particles outside the doubly magic $^{146}_{64}$Gd$_{82}$ core, shows properties of a weakly deformed "transitional" nucleus at low spin and has been discussed [29] in the context of the interacting boson model (IBM). For instance, the $E(4_1^+)/E(2_1^+)$ energy ratio is 2.32, near the O(6) limit of 2.5 for a γ-soft rotor, as opposed to 3.33 for a good rotor [SU(3) limit]. In addition, the bandheads of so-called β- and

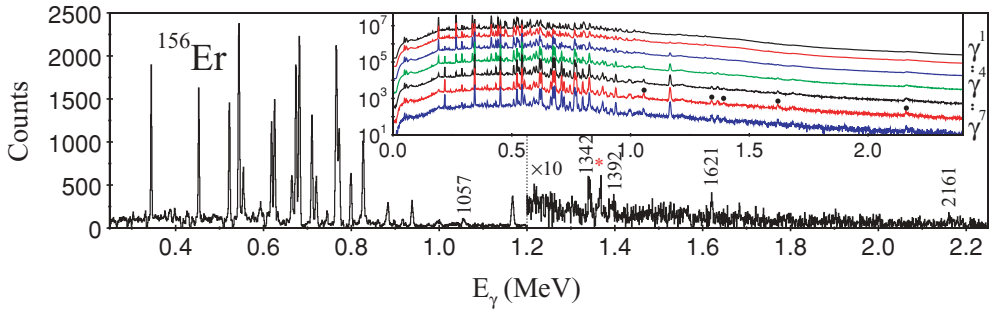

FIG. 4. (Color online) Multiply gated γ-ray spectra obtained from a high-fold analysis of the data for the positive-parity bands in ^{156}Er. The main spectrum represents a γ^6-gated spectrum (i.e., γ^7 analysis) where a corresponding γ^4-gated spectrum (γ^5) has been used as a background spectrum. Note that above 1.2 MeV, the y axis has been scaled by a factor of 10. The inset shows the raw multiply gated spectra from γ^1 (i.e., no gates) up to γ^7 (six gates), plotted logarithmically. The gate list included all the clean gates from the positive-parity structures in ^{156}Er, namely bands 1–3. The five transitions that directly feed the terminating $I^\pi = 42^+$ state are labeled by their energies in keV in the main diagram and denoted by solid circles in the γ^6 inset spectrum. The 1367-keV ($38^+ \rightarrow 36^+$) transition, lying between the newly identified 1342- and 1392-keV transitions is labeled by the (red) asterisk in the main spectrum.

γ-vibrational bands are degenerate, to within 1 keV, at an excitation energy of 930 keV [28] and lie close to the 4_1^+ energy, with $E(0_2^+)/E(4_1^+) = E(2_2^+)/E(4_1^+) = 1.17$ as expected for a U(5) vibrator. Recent theoretical work has also focused on γ-vibrational bands in light erbium isotopes [30] and the fact that they are predicted to become close to yrast at high spin.

Theoretical single-neutron and single-proton energies are shown in Fig. 6 as a function of quadrupole deformation ε_2. They were calculated by using a modified harmonic-oscillator potential with the $A = 150$ parameters [31], with the assumption that the hexadecapole deformation ε_4 is related to the quadrupole deformation ε_2 as $\varepsilon_4 = \varepsilon_2^2/6$. For prolate shape ($\varepsilon_2 \sim 0.2$) in ^{156}Er, the $N = 88$ Fermi level lies below the first $N_{\rm osc} = 6\,(\nu i_{13/2})$ intruder orbital and above the first three $N_{\rm osc} = 5\,(\nu f_{7/2}/h_{9/2})$ orbitals. For oblate shape ($\varepsilon_2 \sim -0.2$), the $N = 88$ Fermi level lies above the first $\nu f_{7/2}$, $\nu h_{9/2}$, and $\nu i_{13/2}$ orbitals. The relevant high-j orbitals near the $Z = 68$ Fermi surface arise from states from the middle of the $N_{\rm osc} = 5$ subshell ($\pi h_{11/2}$) and from states at the top of the $N_{\rm osc} = 4$ subshell ($\pi d_{5/2}/g_{7/2}$ and $d_{3/2}$).

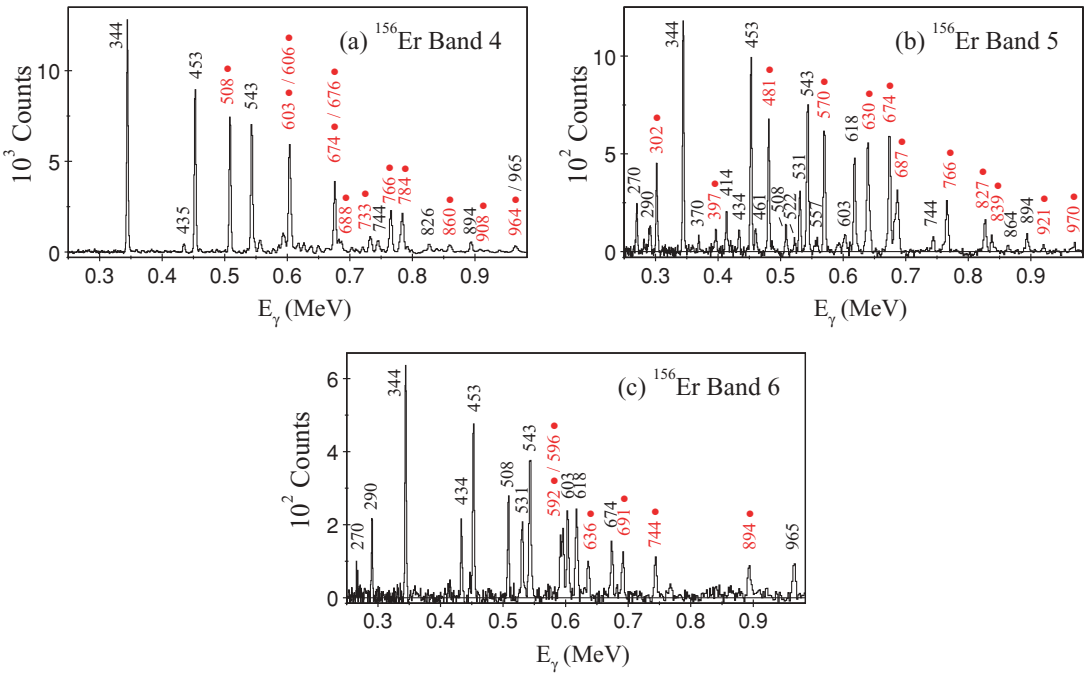

FIG. 5. (Color online) Triple-gated (x, y, z) quadruple-coincidence spectra obtained from the hypercube showing the negative-parity bands in ^{156}Er. (a) Spectrum ($x = 618$, $y = 531$, $z = 434$ keV) showing transitions in band 4 (red) labeled with •; (b) spectrum ($x = 704$, $y = 766$, $z = 683$ keV) showing transitions in band 5 (red) labeled with •; (c) spectrum ($x = 788$, $y = 650$, $z = 617$ keV) showing transitions in band 6 (red) labeled with •.

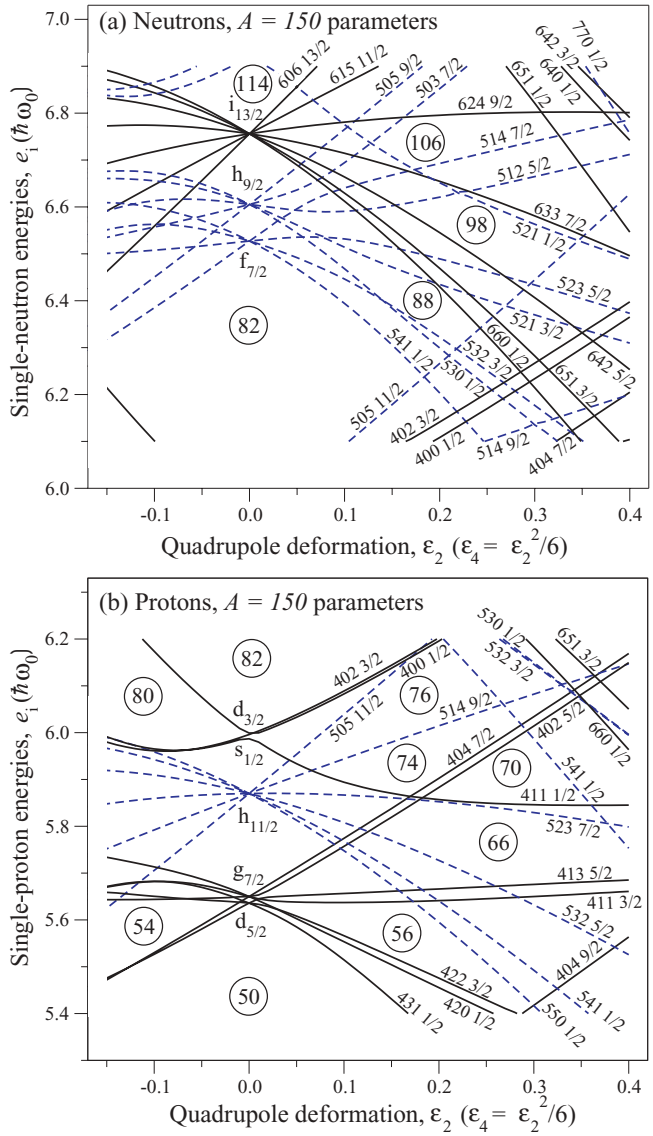

FIG. 6. (Color online) Theoretical single-neutron (a) and single-proton (b) energies, calculated with the $A = 150$ parameters [31], shown as a function of quadrupole deformation. Positive-parity levels are denoted by solid (black) lines and negative-parity levels by dashed (blue) lines, respectively. The levels are labeled by asymptotic quantum numbers $Nn_3\Lambda\Omega$. With the $A = 150$ parameters, the spherical proton $g_{7/2}$, $d_{5/2}$ and $d_{3/2}$, $s_{1/2}$ subshells, respectively, are degenerate, but to make the figure easier to read the $N = 4$ proton κ value has been increased, leading to a small energy split between these subshells.

A. Alignment properties of the bands

To investigate the rotational properties of the bands in ^{156}Er, the experimental alignments [32],

$$i_x(\omega) = I_x(\omega) - I_{x,\mathrm{ref}}(\omega), \tag{2}$$

are shown in Fig. 7, plotted as a function of rotational frequency, $\omega = E_\gamma/\Delta I_x \approx E_\gamma/2\hbar$. At a given spin I, the aligned spin is $I_x = \sqrt{I(I+1) - K^2}$, whereas the rotational

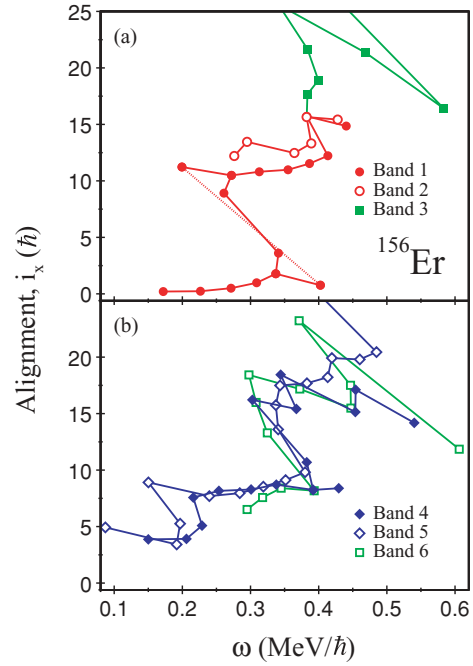

FIG. 7. (Color online) Experimental alignments, i_x, as a function of rotational frequency, ω, for (a) positive-parity bands and (b) negative-parity bands in ^{156}Er.

reference, $I_{x,\mathrm{ref}}$, is given by

$$I_{x,\mathrm{ref}}(\omega) = \omega(\mathcal{J}_0 + \mathcal{J}_1\omega^2) - i_0. \tag{3}$$

Harris parameters [33] $\mathcal{J}_0 = 32.1\hbar^2$ MeV^{-1} and $\mathcal{J}_1 = 34.0\hbar^4$ MeV^{-3}, obtained from ^{157}Ho [34], have been used together with an offset $i_0 = 4.4\hbar$ to ensure that the ground-state band of ^{156}Er has approximately zero alignment at low rotational frequency.

1. Positive-parity bands 1–3

Band 1 shows a sharp backbend at $\omega \approx 0.30$ MeV/$\hbar$ in Fig. 7(a) with an increase in alignment $\Delta i_x \approx 10\hbar$. Such a gain in alignment is consistent with the Coriolis-induced breaking of the first pair of $i_{13/2}$ neutrons, usually referred to as the AB alignment. Band 1a may thus be associated with such a two-quasineutron configuration. The other positive-parity band (band 2) shows an alignment $1\hbar$–$2\hbar$ higher than band 1a. A pure two-quasiparticle configuration cannot generate such a high value of alignment and a four-quasiparticle configuration is not expected at such low spin. Therefore, other mechanisms of producing the extra aligned angular momentum are required. The most obvious way to generate the extra alignment is to invoke nuclear collective modes of excitation. For example, band 2 could be interpreted as the coupling of the AB two-quasineutron structure to the γ vibration of the core. Indeed, as mentioned previously, γ-vibrational bands are predicted to approach yrast in the light erbium isotopes at high spin [30].

Bands 1 and 2 show a further irregularity, or band crossing, at $\omega \approx 0.39$ MeV/$\hbar$, where band 3 becomes yrast. The alignment properties of band 3 are not consistent with well-behaved rotational motion and rather suggest noncollective

behavior beyond $\omega = 0.40$ MeV/$\hbar$. Indeed, this band has previously been discussed in terms of a weakly deformed triaxial-oblate terminating configuration [7,10]. Furthermore, lifetime measurements of the high-spin positive-parity levels in ^{156}Er [21] support this interpretation of a dramatic loss of collectivity at high spin.

2. *Negative-parity bands 4–6*

The negative-parity bands 4–6 all show an experimental alignment $i_x \approx 7\hbar$ [see Fig. 7(b)] in the frequency range $0.25 < \omega < 0.40$ MeV/$\hbar$. Such a value is consistent with a two-quasineutron configuration formed by coupling a single $i_{13/2}$ neutron to the available negative-parity orbitals, originating from the $\nu h_{9/2}$ and $\nu f_{7/2}$ states. This type of structure is further corroborated by the absence of a backbend at $\omega \approx 0.30$ MeV/$\hbar$, seen in the positive-parity structures, resulting from Pauli blocking of the $\nu i_{13/2}$ orbital. Moreover, negative-parity two-quasiproton configurations, formed by coupling $\pi h_{11/2}$ and $\pi g_{7/2}/d_{5/2}$ states, can also be ruled out by similar arguments; these *proton* bands would be expected to show the AB neutron alignment at $\omega \approx 0.30$ MeV/$\hbar$.

With reference to Fig. 6(a), prolate negative-parity two-quasineutron configurations can be formed in $^{156}_{68}$Er$_{88}$ by coupling $[530]1/2^-$ and $[532]3/2^-$ Nilsson levels, below $N = 88$, to the $[660]1/2^-$ intruder, above $N = 88$, yielding structures with $K^\pi = 1^-$ and 2^-, respectively. Indeed, the $K^\pi = 1^-$ configuration has been predicted to be yrast at low spin by using a particle-number projected Hartree-Fock-Bogoliubov treatment [35]. At low frequency, $\omega \sim 0.20$ MeV/$\hbar$, bands 4 and 5 undergo a backbend into bands 4a and 5a, respectively, with an increase of $\approx 4\hbar$ of alignment [see Fig. 7(b)]. The low-spin configurations of bands 4 and 5 involve fully paired, zero-quasiparticle states of possible collective nature. For example, octupole collectivity would yield negative-parity bands with an alignment of $3\hbar$, consistent with that of bands 4 and 5 below $\omega = 0.20$ MeV/$\hbar$.

All three negative-parity bands show a band-crossing at $\omega \approx 0.35$ MeV/$\hbar$. The large gain in alignment, taken with the low crossing frequency, suggest that this is unlikely to be due to further $\nu i_{13/2}$ alignment (BC); the position of the $N = 88$ neutron Fermi resides below the $\nu i_{13/2}$ shell [see Fig. 6(b)]. At higher spin/frequency all three negative-parity bands show irregular behavior, similar to the positive-parity structures at high spin, which again suggests a major change in shape to weakly deformed oblate-triaxial.

B. Comparison with $N = 88$ isotones

Experimental alignments are shown in Fig. 8 for bands with parity and signature $(\pi, \alpha) = (+, 0)$ in the $N = 88$ isotones ^{152}Gd [36], ^{154}Dy [37], ^{158}Yb [5,38,39], ^{160}Hf [40,41], and ^{162}W [41,42], calculated by using the same reference as in Fig. 7. All isotones show evidence for the rotational alignment of a quasiparticle pair at similar frequencies. In the case of the lightest two isotones, namely ^{152}Gd and ^{154}Dy, there are two positive-parity bands, as shown in Fig. 8(a). The ground-state bands, labeled 1, show very similar behavior with a gradual increase of alignment over a wide frequency range. The second

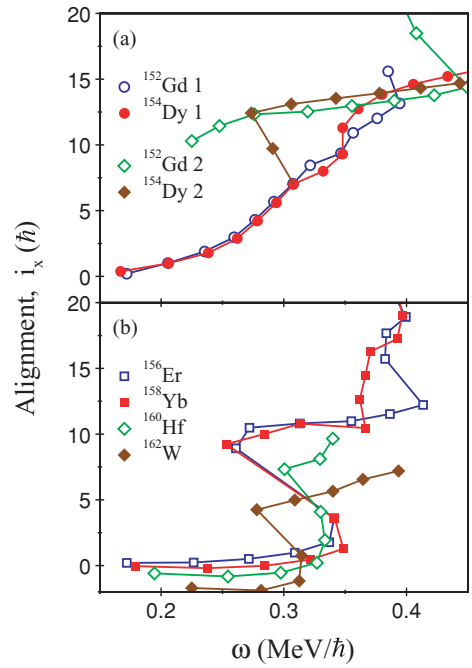

FIG. 8. (Color online) Experimental alignments, i_x, as a function of rotational frequency, ω, for $(\pi, \alpha) = (+, 0)$ bands in $N = 88$ isotones.

bands, labeled 2, appear to show a weak interaction with the ground-state bands and indeed a sharp backbend is seen in the case of ^{154}Dy. The alignments of ^{156}Er and ^{158}Yb, shown in Fig. 8(b), also follow each other closely and exhibit a sharp backbend at $\omega = 0.30$ MeV/$\hbar$. The heaviest isotones, ^{160}Hf and ^{162}W, also show sharp backbends but with a reduced gain in alignment Δi_x. Furthermore, the backbend in ^{160}Hf occurs at an unusually high frequency compared with the other isotones.

These observations suggest that more than one type of quasiparticle may be responsible for the observed behavior. For instance, competition between the rotational alignments of $\nu h_{9/2}$ and $\nu i_{13/2}$ quasiparticle pairs may explain the alignment properties shown in Fig. 8. For example, the low alignment gain in ^{162}W has been attributed to $\nu h_{9/2}$ rather than $\nu i_{13/2}$ quasiparticles [42].

The lighter $N = 88$ isotones ^{152}Gd [36] and ^{154}Dy [37] exhibit strongly coupled sidebands built on configurations with a single neutron hole in the $h_{11/2}$ subshell, corresponding to the high-K $[505]11/2^-$ Nilsson state of Fig. 6(a). Such a structure was not however observed in the present analysis of ^{156}Er. Furthermore, no strongly coupled bands have been observed in the heavier ^{158}Yb [5,38,39], ^{160}Hf [40,41], and ^{162}W [41,42] isotones, although similar high-K structures have been observed in the heavier erbium isotopes [43]. These observations are consistent with reduced quadrupole deformation in ^{156}Er compared with heavier isotopes but lighter isotones; predicted [44] quadrupole deformation parameters for $N = 88$ isotones are listed in Table III.

C. Links between the bands in ^{156}Er

Many new $\Delta I = 1$ intraband transitions have been established between the $\Delta I = 2$ bands in ^{156}Er from the present

TABLE III. Predicted [44] ground-state deformation parameters for $N = 88$ isotones. The lightest two isotones have nonzero values of octupole deformation, ε_3.

Isotone	ε_2	ε_3	ε_4
$^{144}_{56}$Ba	0.150	0.091	−0.053
$^{146}_{58}$Ce	0.167	0.084	−0.053
$^{148}_{60}$Nd	0.192		−0.053
$^{150}_{62}$Sm	0.192		−0.040
$^{152}_{64}$Gd	0.192		−0.027
$^{154}_{66}$Dy	0.192		−0.020
$^{156}_{68}$Er	0.175		−0.013
$^{158}_{70}$Yb	0.150		−0.020
$^{160}_{72}$Hf	0.142		−0.013
$^{162}_{74}$W	0.125		−0.007
$^{164}_{76}$Os	0.100		0.007
$^{166}_{78}$Pt	−0.067		0.007

data. The observation of such transitions readily allows an estimation of ratios of reduced transition probabilities from measured γ-ray intensity ratios that depopulate levels; these include $B(M1; I \to I-1)/B(E2; I \to I-2)$ and $B(E1; I \to I-1)/B(E2; I \to I-2)$ ratios. In the present analysis, double- or triple-gated γ-ray spectra were produced using gates above the level of interest. The intensity branching ratio, $\lambda \equiv I_\gamma(\Delta I = 1)/I_\gamma(\Delta I = 2)$, of the competing dipole and quadrupole transitions depopulating that level was then measured.

The $B(M1; I \to I-1)/B(E2; I \to I-2)$ and $B(E1; I \to I-1)/B(E2; I \to I-2)$ ratios of reduced transition probabilities were determined as

$$\frac{B(M1)}{B(E2)} = \frac{\lambda}{1.43 \times 10^4} \frac{[E_\gamma(\Delta I = 2)]^5}{[E_\gamma(\Delta I = 1)]^3} \left(\mu_N^2\ e^{-2}\ \mathrm{fm}^{-4}\right) \quad (4)$$

and

$$\frac{B(E1)}{B(E2)} = \frac{\lambda}{1.30 \times 10^6} \frac{[E_\gamma(\Delta I = 2)]^5}{[E_\gamma(\Delta I = 1)]^3}\ (\mathrm{fm}^{-2}), \quad (5)$$

respectively, with γ-ray energies in MeV. The $\Delta I = 1$ transitions were assumed to be pure stretched dipole in character with no quadrupole admixture (i.e., with a multipole mixing ratio $\delta \equiv 0$). For nonzero δ, Eqs. (4) and (5) should be modified by a factor $(1 + \delta^2)^{-1}$ but are insensitive to δ since typically $\delta^2 \ll 1$. Moreover, the errors introduced by the experimental branching ratios λ are usually significantly larger than the effect of neglecting δ, particularly in the present case where the relevant dipole transitions are weak.

$B(M1)$ and $B(E1)$ strengths have also been extracted by using the following expression as an estimate for the $B(E2)$ rate:

$$B(E2; I \to I-2) = \frac{5}{16\pi} Q_0^2\, |\langle I\,K\,20 | I-2\,K\rangle|^2\,, \quad (6)$$

obtained from the rotational model [45]. An average quadrupole moment of $Q_0 = 440\ e\ \mathrm{fm}^2$ has been used to determine the $B(E2)$ values. This value of quadrupole moment was determined from the predicted average quadrupole deformation of $\varepsilon_2 = 0.175$ for ^{156}Er at low spin [44].

1. $B(M1)/B(E2)$ ratios

Measured $B(M1)/B(E2)$ ratios for transitions between bands 5 and 4, and for transitions between bands 6 and 5, are listed in Table IV, together with estimated $B(M1)$ strengths. The deduced $B(M1)$ values are all rather low for transitions

TABLE IV. Experimental $B(M1)/B(E2)$ ratios of reduced transition probabilities and deduced $B(M1)$ strengths in ^{156}Er.

I	$E_\gamma(I \to I-1)$ (keV)	$E_\gamma(I \to I-2)$ (keV)	Branching ratio λ $I_\gamma(M1)/I_\gamma(E2)$	$B(M1)/B(E2)$ ($10^{-6}\ \mu_N^2\ e^{-2}\ \mathrm{fm}^{-4}$)	$B(M1)$ ($10^{-2}\ \mu_N^2$)	$B(M1)$ (10^{-2} W.u.)[a]
			Band 5 → Band 4			
6	592	390	1.7(3)	5.2(9)	3.4(6)	1.9(3)
10	414	302	0.42(2)	1.0(1)	0.7(1)	0.4(1)
12	461	481	0.11(1)	2.1(2)	1.4(1)	0.8(1)
14	522	570	0.06(2)	1.8(5)	1.1(3)	0.7(2)
16	557	639	0.09(2)	4(1)	2.7(7)	1.5(4)
18	585	704	0.17(3)	10(2)	7(2)	4(1)
22	385	683	0.19(3)	3.4(7)	2.2(4)	1.2(2)
22	480	683	0.97(9)	91(9)	59(6)	33(3)
			Band 6 → Band 5			
13	290	592	0.08(2)	16(5)	10(4)	6(2)
15	356	636	0.15(7)	24(11)	15(7)	8(4)
17	408	691	0.11(4)	17(6)	11(4)	6(2)
19	491	788	0.32(7)	58(13)	38(9)	21(5)
21	378	650	0.22(5)	47(11)	30(7)	17(4)
25	235	596	0.29(7)	115(27)	75(18)	42(10)

[a] 1 W.u. = 1.79 μ_N^2.

between these two-quasineutron bands, as expected since they are based on low-Ω Nilsson orbitals from the bottom of the $\nu i_{13/2}$, $\nu h_{9/2}$, and $\nu f_{7/2}$ subshells. There is however a clear difference in the values extracted for transitions between bands 5 and 4 compared with those between bands 6 and 5; the latter $B(M1)$ values are up to an order of magnitude larger. This may suggest that bands 5 and 6 are signature partners based on the same intrinsic negative-parity neutron configuration (e.g., $\nu i_{13/2} f_{7/2}$), whereas band 4 contains a different orbital (e.g., $\nu i_{13/2} h_{9/2}$).

The 22^- state of band 5b decays into both the 21^- state of band 4a, through a 385-keV transition, and also the 21^- state of band 4b, through a 480-keV transition. There is a significant difference of a factor of ∼30 in the $B(M1)$ strengths for these decays. The strong connection (band 5b → 4b) occurs between bands that both exist above the crossing evident in Fig. 7(b). In contrast, the weak connection (band 5b → 4a) occurs from a band above this crossing, into a band below the crossing.

2. $B(E1)/B(E2)$ ratios

Measured $B(E1)/B(E2)$ ratios for transitions between bands 4 and 1, and for transitions between bands 2 and 4, are listed in Table V, together with estimated $B(E1)$ strengths. The deduced $B(E1)$ values are of the order of 10^{-3} W.u. between bands 4 and 1. The observation of such high $B(E1)$ strength [usually taken as $B(E1) > 10^{-5}$ W.u.] is often cited as evidence for octupole correlations in nuclei [46]. These correlations break reflection symmetry and may be either static (deformation) or dynamic (vibrational) in nature. In this mass region, octupole collectivity may be expected since both proton ($h_{11/2}$ and $d_{5/2}$) and neutron ($i_{13/2}$ and $f_{7/2}$) orbitals with $\Delta N_{\rm osc} = 1$ and $\Delta j = \Delta l = 3$ are near the Fermi surface.

The role of octupole collectivity in the neutron-rich "barium region," including the lighter $N = 88$ isotones ranging from $^{142}_{54}$Xe up to $^{152}_{64}$Gd, has been investigated [47] using a cranking model with an axial Woods-Saxon single-particle potential with pairing [48,49]. It was found that the $^{148}_{60}$Nd, $^{150}_{62}$Sm, and $^{152}_{64}$Gd isotones can best be described as nuclei with well-developed quadrupole (β_2) deformation in their ground states, but with a softness with respect to octupole deformation (β_3) centered around the reflection-symmetric shape, $\beta_3 = 0$. The light $N = 88$ isotones may thus be susceptible to dynamic octupole vibrations at low spin. However, at medium spin/frequency values, static octupole-deformed shapes with $\beta_3 \neq 0$ develop, but these return to reflection-symmetric shapes with increasing spin [47]. An alternative approach was considered by Skalski [50], who introduced coupling between γ (nonaxial) deformation and β_3 (reflection-asymmetric) degrees of freedom in the "triaxial-octupole" description of the level structure of ^{148}Sm (Y_3^μ tensor). A similar approach is probably warranted for ^{156}Er.

D. High-spin behavior: cranked Nilsson-Strutinsky calculations

To address the high-spin behavior of ^{156}Er, theoretical calculations have been performed in the framework of the configuration-dependent cranked Nilsson-Strutinsky (CNS) formalism without pairing [11,51]. For the κ and μ parameters defining the **l.s** and $\mathbf{l}^2$ strengths of the modified oscillator potential, $A = 150$ parameters [31] have been used (see Fig. 6).

In the theoretical results presented in the following sections, absolute energies at high spin are calculated [52] based on the Lublin-Strasbourg drop (LSD) model [53] and a rigid moment of inertia calculated with a radius parameter $r_0 = 1.16$ fm and a diffuse surface [54]. Theoretical configurations are labeled using the short-hand notation $[p_1(p_2 p_3), (n_1 n_2) n_3]$, where p_1 represents the number of $\pi h_{11/2}$ particles and n_3 the number of $\nu i_{13/2}$ particles. The other labels, in parentheses, are only used if nonzero: p_2 and p_3 represent the number of protons of $h_{9/2}/f_{7/2}$ and $i_{13/2}$ character, respectively; n_1 and n_2 represent the number of neutron holes of $N_{\rm osc} = 4$ and $h_{11/2}$ character, respectively. The configurations may be written in full as

$$\pi\{(h_{11/2})^{p_1}(h_{9/2}/f_{7/2})^{p_2}(i_{13/2})^{p_3}\} \otimes \nu\{(N_{\rm osc}=4)^{-n_1}(h_{11/2})^{-n_2}(i_{13/2})^{n_3}\}.$$

To obtain a general overview of favored coupling schemes at different spin values, calculated potential-energy surfaces for $(\pi, \alpha) = (+, 0)$ states in ^{156}Er are presented in Fig. 9. These energy surfaces suggest that, for low-spin values, the yrast states should correspond to normal-deformed bands that are, on average, prolate but soft toward γ deformation (i.e., triaxiality). However, for spin values approaching $I = 40$, a

TABLE V. Experimental $B(E1)/B(E2)$ ratios of reduced transition probabilities and deduced $B(E1)$ strengths in ^{156}Er.

I	$E_\gamma(I \to I-1)$ (keV)	$E_\gamma(I \to I-2)$ (keV)	Branching ratio λ $I_\gamma(E1)/I_\gamma(E2)$	$B(E1)/B(E2)$ (10^{-7} fm^{-2})	$B(E1)$ (10^{-3} e^2 fm^2)	$B(E1)$ (10^{-3} W.u.)[a]
			Band 4 → Band 1			
7	689	417	10(1)	3.1(5)	2.0(3)	1.1(2)
9	531	461	3.8(1)	4.0(2)	2.6(1)	1.4(1)
11	290	434	0.64(2)	3.1(1)	2.1(1)	1.1(1)
			Band 2 → Band 4			
18	627	556	0.49(5)	1.1(2)	0.7(2)	0.4(1)
20	435	593	1.3(8)	8.8(6)	5.7(4)	3.0(2)
22	307	732	0.23(8)	13(5)	8(3)	4(2)

[a]1 W.u. = 1.87 e^2 fm^2.

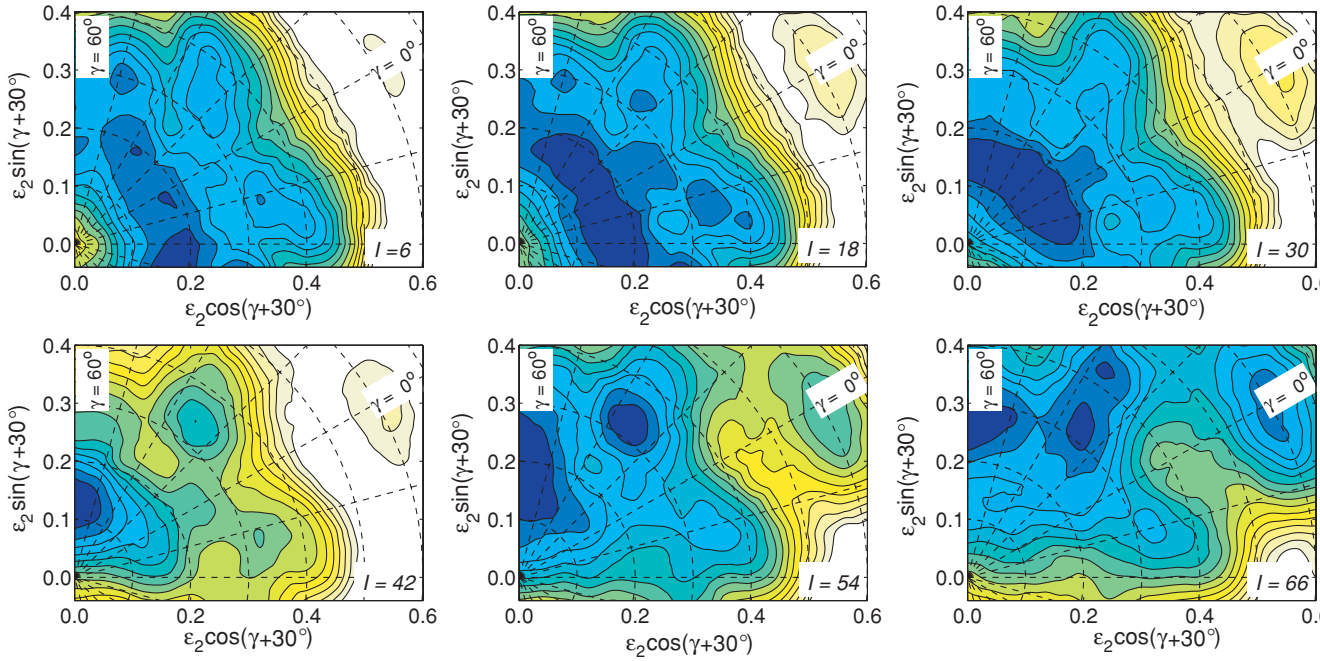

FIG. 9. (Color online) Calculated potential energy surfaces of ^{156}Er with $(\pi, \alpha) = (+, 0)$ for spin values $I = 6$, 18, 30, 42, 54, and 66. The contour lines are separated by 0.5 MeV, with darker shades (blue) lower in energy than lighter shades (green-yellow).

transition to noncollective oblate states ($\gamma = 60°$) is calculated and it appears that such oblate states are competitive in energy up to very high spin, $I \approx 70$, with a small increase of ε_2 deformation with increasing spin. Also, over a large spin range, an energy minimum at $\varepsilon_2 = 0.3$–0.4 and $\gamma \approx 20°$ (triaxial strongly deformed, TSD) is calculated to be approximately 1 MeV above yrast; this minimum becomes yrast or very close to yrast for $I = 50$–60. For low- and intermediate-spin values, there is also a competition from a negative-γ energy minimum, corresponding to the same configuration but with rotation around the intermediate principal axis (with positive γ corresponding to rotation around the shortest principal axis). Finally, for spin values $I = 60$ and above, a superdeformed (SD) minimum at $\varepsilon_2 \approx 0.6$, $\gamma \approx 0°$ is calculated to be low in energy.

1. *Positive-parity states*

The observed positive-parity states in ^{156}Er for $I > 30$ spin are shown relative to a rotating liquid-drop reference in Fig. 10, where they are compared with the CNS calculations. As previously proposed in Ref. [7], and furthermore supported by calculations in Refs. [8,9], the positive-parity yrast band appears to terminate into an energetically favored state at $I = 42$. When drawn relative to the rotating liquid-drop energy [see Fig. 10(a)], this $I = 42$ state is strongly favored in energy and the band is sloping downward for spin values above $I = 30$. Termination at $I = 42$ is expected since this is the highest spin that can be formed in ^{156}Er, with positive parity, from the four valence protons and six valence neutrons outside the ^{146}Gd core. The filling of the valence orbitals in the fully aligned $I = 42$ state is illustrated in the tilted Fermi surface diagram [55] of Fig. 11 appropriate for ^{156}Er. The configuration of the terminating state may be written in full as

$$\pi\left\{(h_{11/2})^4_{16}\right\}_{16^+} \otimes \nu\left\{(i_{13/2})^2_{12}(h_{9/2}/f_{7/2})^4_{14}\right\}_{26^+}.$$

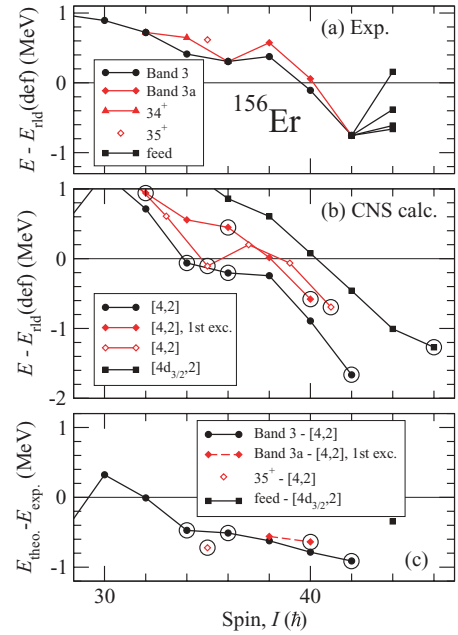

FIG. 10. (Color online) (a) The observed positive-parity states in the $I > 30$ spin range of ^{156}Er shown relative to a rotating liquid drop reference. The low-lying calculated states are shown relative to the same reference in (b), with the difference between experiment and calculations shown in (c). Calculated noncollective aligned states are encircled.

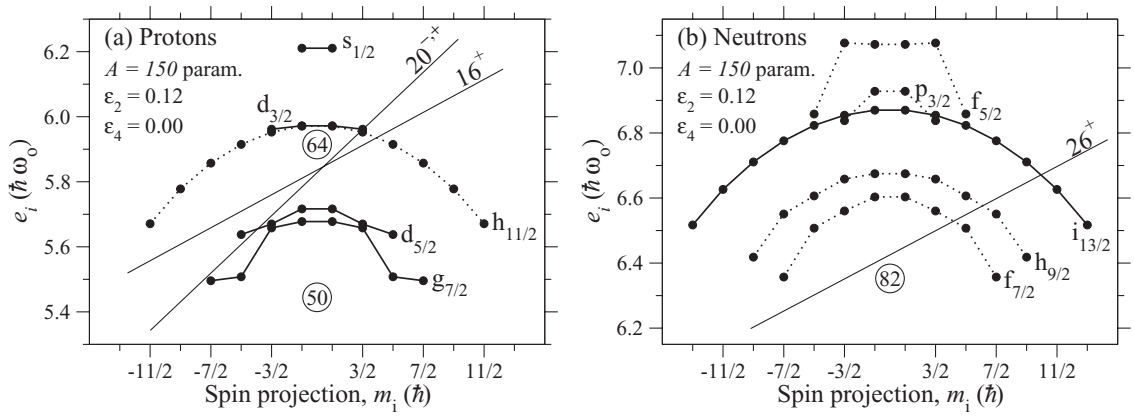

FIG. 11. Tilted-Fermi-surface diagrams for (a) protons and (b) neutrons at oblate shape, showing the configurations of the calculated yrast $I^\pi = 42^+$ and $I^\pi = 46^\pm$ terminating states in ^{156}Er, built from 16^+ and $20^\pm$ proton configurations coupled to a 26^+ neutron configuration.

The corresponding calculated band, which is illustrated in Fig. 10(b), also shows a strong downward slope in the $I = 30$–40 range with a strongly favored $I = 42$ state. The difference between experiment and calculations is drawn in Fig. 10(c), which shows a rather constant value of ∼0.7 MeV for spin values $I = 34$–42, with values closer to zero for $I = 30$–32. It is evident that, in both experiment and theory, the energies for $I = 34$–36 are lower than expected from a smooth trend. In the calculations, these states are formed at oblate shape with the spin vector of a valence neutron and a valence proton, respectively, in the opposite direction relative to the total spin vector [8,9]. Thus, relative to the fully aligned $I = 42$ state, one $f_{7/2}/h_{9/2}$ neutron is shifted from an $m_i = 5/2$ to an $m_i = -7/2$ orbital and one $h_{11/2}$ proton from an $m_i = 5/2$ to an $m_i = -11/2$ orbital, respectively. Similarly, a relatively low lying $I = 35$ state is calculated in which, relative to the fully aligned $I = 42$ state, one $f_{7/2}/h_{9/2}$ neutron is shifted from an $m_i = 7/2$ to an $m_i = -7/2$ orbital. This $I = 35$ state shows up as clearly most favored in the odd-spin [4, 2] sequence drawn in Fig. 10(b) and it is very satisfying that the only positive-parity odd-spin state that has been observed [7] in the $I = 30$–42 spin range indeed has $I = 35$.

In the experimental level scheme there are also relatively low lying excited $I = 40$ and $I = 38$ states, referred to as band 3a in Fig. 3. In calculations, the [4, 2] configuration is clearly favored around $I = 40$, as discussed in more detail in the following. Therefore, it seems very unlikely that the observed states in band 3a are formed in any other configuration. However, other low-lying bands can be formed within the [4, 2] configuration. Because the $Z = 64$ proton core is closed and the two lowest $i_{13/2}$ neutron orbitals are strongly favored, low-energy excitations must involve the $f_{7/2}/h_{9/2}$ neutron orbitals. To describe these excited bands, the orbitals are labeled as belonging to $f_{7/2}$ and $h_{9/2}$, respectively, in accordance with Fig. 11, although the $f_{7/2}$ and $h_{9/2}$ subshells are in reality strongly mixed. The $f_{7/2}/h_{9/2}$ component of the lowest band illustrated in Fig. 11 would then be labeled as $\{(f_{7/2})^2_6(h_{9/2})^2_8\}_{14^+}$. Other bands are then formed as $\{(f_{7/2})^1_{7/2}(h_{9/2})^3_{21/2}\}_{14^+}$ (shifting an $m_i = 5/2\, f_{7/2}$ neutron to an $m_i = 5/2\, h_{9/2}$ state) and $\{(f_{7/2})^3_{15/2}(h_{9/2})^1_{9/2}\}_{12^+}$ (shifting an $m_i = 7/2\, h_{9/2}$ neutron to an $m_i = 3/2\, f_{7/2}$ state). When combined with the other particles in the [4, 2] configuration, excited bands terminating at $I = 42$ and $I = 40$, respectively, are formed. The band terminating at $I = 40$ comes lowest in energy and only this band is drawn in Fig. 10(b). If this excited [4, 2] band is assigned to the observed band 3a, the agreement between experiment and calculations is excellent for the relative energies of the two $I = 40$ and the two $I = 38$ states, respectively. However, a relatively low lying second $I = 34$ state has also been observed and, in this case, the lowest excited $I = 34$ state is calculated to be considerably higher in energy.

2. *Beyond valence-space band termination: core-excited states*

Experimentally, there are four $I^\pi = 44^+$ states that have been observed feeding the valence-space aligned $I^\pi = 42^+$ state, with three of them very close in energy and the fourth somewhat higher (see Fig. 3). In the CNS calculations, the lowest energy (yrast) $I = 44$ state is formed in the configuration with one proton excited across the $Z = 64$ gap, as illustrated in Fig. 11(a). This is a [4, 2] configuration but, because it has one proton in a $d_{3/2}$ orbital, it is referred to as $[4d_{3/2}, 2]$. This band has $I_{\max} = 46$, where both the terminating $I = 46$ state and its associated $I = 44$ state are calculated as yrast for positive parity. This theoretical 44^+ state should thus be assigned to the lowest of the observed $I^\pi = 44^+$ states feeding the closed-core $I^\pi = 42^+$ state. However, when comparing experiment with calculations, the $I = 44$ state is calculated to be approximately 0.5 MeV too high relative to the $I = 42$ state [i.e., the transition energy $E_\gamma(44 \to 42)$ is observed at 1.3 MeV and calculated at 1.8 MeV]. Agreement between calculation and experiment would be obtained if the spacing between the $d_{5/2}/g_{7/2}$ and the $d_{3/2}$ subshells was decreased by 500 keV.

In comparing ^{156}Er with ^{157}Er, there is an important difference in that there are three low-lying favored terminating states in ^{157}Er at similar excitation energies [15,16], but only one in ^{156}Er. Therefore, in ^{157}Er, excited states can be built

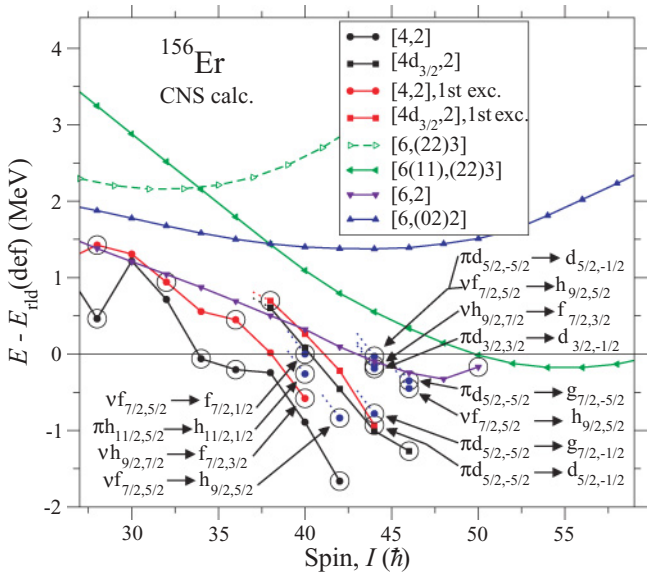

FIG. 12. (Color online) Energies of calculated bands in ^{156}Er relative to a rotating liquid-drop reference. Bands terminating at $I = 42$([4, 2] configuration with no $d_{3/2}$ proton) and $I = 46$ ([4, 2] configuration with one $d_{3/2}$ proton) are included, together with the first-excited bands built on these states. Noncollective aligned states are encircled. Other aligned excited states at $I = 42$–46 are drawn and the corresponding terminating bands are indicated schematically. For these aligned states, it is specified which particle, labeled by its angular momentum j and projection m_i, is excited relative to the aligned $I = 42$ and $I = 46$ states, respectively. The labeling of the orbitals is defined in Fig. 11, where it should be noted that this labeling only reflects one j shell, which has a large component in the wave function. Calculated bands of different collectivity are also included and become yrast for some spin values above $I = 50$.

on all three states, making many more possibilities to form low-lying states of different signature and parity that can feed the aligned states. In ^{156}Er, there is only one band with positive parity and even spins (signature $\alpha = 0$) that is calculated to be reasonably low in energy for spin values $I^\pi = 44^+, 46^+$, namely the configuration terminating at $I = 46$ drawn in Fig. 10(b). As illustrated in Fig. 12, the band that has two $d_{5/2}/g_{7/2}$ protons excited to $h_{11/2}$ orbitals appears around 1 MeV higher in energy. However, it is also illustrated in Fig. 12 how several excited bands at a relatively low energy can be formed within the configuration terminating at $I = 46$.

To understand possible configurations of the states feeding the $I = 42$ state, it is instructive to first consider possible excitations within the closed-core configuration. The building of this $I^\pi = 42^+$ state is illustrated in Fig. 11. For the protons, it is only possible to shift positions of the $h_{11/2}$ particles, which leads to rather unfavored energies. For example, the $m_i = 5/2$ particle can move to the $m_i = 1/2$ state, but this leads to an $I = 40$ state at a higher energy than the original $I = 42$ state. Thus, with the reference subtracted, this $I = 40$ state appears at a high energy in Fig. 12. To form lower excited states, excitations within the neutrons should be considered, where the most important excitations lead to aligned $I = 40$ and $I = 42$ states discussed above and shown in Fig. 12. Within this configuration, there are no more $I = 42$ states, but it is also illustrated in Fig. 12 how it is possible to form an excited $I = 40$ state when an $f_{7/2}$ neutron is shifted to an orbital with lower alignment ($m_i = 5/2 \rightarrow 1/2$) in a similar way as discussed for the $h_{11/2}$ proton above.

The configuration terminating at $I = 46$, which has one proton excited from $d_{5/2}/g_{7/2}$ to $d_{3/2}$ states relative to the closed-core configuration, will now be discussed. In this case, the hole in the $d_{5/2}/g_{7/2}$ state leads to more possibilities of forming low-lying excited states. In particular, it becomes possible to form two aligned $I = 44$ states at a lower energy than the terminating $I = 46$ state by shifting the $m_i = -5/2\, d_{5/2}$ particle to the $m_i = -1/2\, d_{5/2}$ and $g_{7/2}$ states, respectively. When drawn relative to the reference, these aligned $I = 44$ states lie just above the slightly collective $I = 44$ state, which belongs to the band that terminates at $I = 46$. The presence of these three low-lying calculated $I = 44$ states is then consistent with the three relatively low-lying $I^\pi = 44^+$ states, which are observed to feed the closed-core $I^\pi = 42^+$ state (see Fig. 3). The next $I = 44$ and 46 states are then calculated at a considerably higher energy. Note especially that the first aligned $I = 44$ state based on neutron excitations is high above the yrast $I = 44$ state, whereas the corresponding $I = 40$ state is rather close to the yrast $I = 40$ state. Indeed, if one neglects small differences in the equilibrium deformations, this $I = 44$ state lies as high above the yrast $I = 46$ state as the $I = 40$ state lies above the yrast $I = 42$ state. However, because the yrast $I = 42$ state is much more favored in energy than the yrast $I = 46$ state, the relative energies of the $I = 44$ and the $I = 40$ states, respectively, come out as very different.

Because all projections of the spin vectors are considered, there might be some spurious components when the aligned states in Fig. 12 are associated with the corresponding spin values. This was discussed for close-to-spherical states built on a few valence particles in Ref. [56]. The problems should be less severe in the present case given the larger deformation with particles distributed over several j shells. For example, the three lowest bands in the closed-core [4, 2] configuration should be fine because they can be labeled as built with a different number of neutrons in the $f_{7/2}$ and $h_{9/2}$ subshells as discussed earlier. The three lowest $I = 44$ states in the configuration terminating at $I = 46$ are more problematic since only two bands could be built from a hole in a spherical $d_{5/2}/g_{7/2}$ configuration. Therefore, if the spurious components were removed, the energies of these states would probably increase somewhat but not in any drastic way given the coupling with the particles in other j shells and the appreciable deformation corresponding to mixed j shells. For the states that are around 1 MeV or more above yrast, the problems with spurious components might become more serious. In any case, however, in this energy range, being able to predict the individual energies for states or bands that reside in the same potential-energy minimum as the yrast states is not expected. In summary, the four experimental $I^\pi = 44^+$ states feeding the closed-core $I^\pi = 42^+$ terminating state in ^{156}Er are predicted to correspond to a one-particle–one-hole excitation across the spherical $Z = 64$ shell gap. The lowest energy such state involves the $\pi d_{5/2}/g_{7/2} \rightarrow \pi d_{3/2}$ excitation, leading to a configuration that terminates at $I = 46$ (i.e., the 44^+ state is the $I_{\max} - 2$ state in this configuration). Several other 44^+ states

are formed from rearrangements of the particles relative to this terminating 46^+ state (i.e., decreasing the m_i value of one particle by $2\hbar$), which means that the spin vector of all these states is aligned along the rotation axis ($\gamma = 60^\circ$). The lowest energy states of this type are obtained from rearrangements within the $\pi d_{5/2}/g_{7/2}$ hole whereas states at a somewhat higher energy are calculated when the particles above the shell gaps are rearranged.

3. Collective bands at high spin

The CNS calculations can be used to search for low-lying bands at different deformations that could be experimentally accessible. For example, by considering $I = 44$ states in other positive-parity configurations than that of the yrast state, the lowest band is formed in the [6, 2] configuration and is calculated to be around 1 MeV above yrast for $I = 44, 46$, as illustrated in Fig. 12. Indeed, it is predicted to have a similar excitation energy in the whole range $I = 34$–46 with the exception of the $I = 42$ state and then it comes very close to yrast for $I = 30$. This band evolves to a smooth termination [4] at $I = 50$, which means that it will be rather collective for spin values $I = 30$–40. Indeed, one could hope to be able to identify coexisting terminating and more-collective bands for $I = 30$–50 in ^{156}Er in a similar way as for the isotone ^{154}Dy [37].

The ^{156}Er nucleus is situated at the lower edge of a mass region with strong evidence for TSD bands at high spin [57]. Such bands have been observed in several erbium isotopes, namely ^{154}Er [58], ^{157,158}Er [26], and recently ^{159,160}Er [59]. The potential energy surfaces of Fig. 9, with a minimum at $\varepsilon_2 \approx 0.35$, $\gamma \approx 20^\circ$, suggest that it should also be possible to observe TSD bands in ^{156}Er. The typical features of such TSD configurations is the presence of two neutron holes in both the $h_{11/2}$ and the $N_{\rm osc} = 4$ orbitals of the $N = 82$ core and, additionally, a few protons in high-j $i_{13/2}$ and $h_{9/2}$ orbitals [26]. The most favored band of this type calculated for ^{156}Er is included in Fig. 12, where it is labeled [6(11), (22)3]. This band is calculated to be yrast or very close to yrast for spin values around or above $I = 50$.

4. Negative-parity states

The observed highest energy states of negative parity are drawn relative to the rotating liquid drop reference in Fig. 13(a). The states for $I > 30$ are rather irregular, suggesting low collectivity, with a low-lying $I^\pi = 38^-$ state, which has previously been interpreted [8,9] as the terminating state of the [4, 1] configuration. Given the calculated low-energy negative-parity states [Fig. 13(b)] and the difference between experiment and calculations [Fig. 13(c)], this appears reasonable. It may however appear strange that it has not been possible to experimentally identify the $I = 39$ state, which is formed in the signature-partner configuration; that is, these terminating $I = 38, 39$ states are formed as $\pi\{(h_{11/2})^4_{16}\}_{16^+} \otimes \nu\{(h_{9/2}f_{7/2})^5_{31/2,33/2}(i_{13/2})^1_{13/2}\}_{22,23^-}$. In the present experiment, the negative-parity sidebands in ^{156}Er were populated weakly and heavily contaminated by overlapping

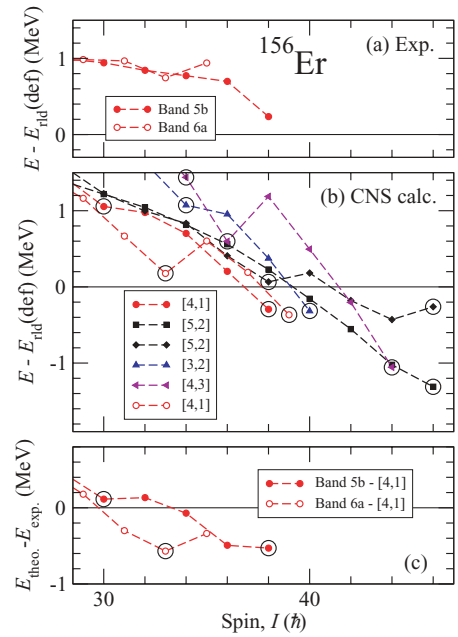

FIG. 13. (Color online) (a) The observed negative-parity states with signature $\alpha = 0$ in the $I > 30$ spin range of ^{156}Er shown relative to a rotating liquid drop reference. The low-lying calculated $\alpha = 0$ states are shown relative to the same reference in (b), including the $\alpha = 1[4, 1]$ band, which is generally calculated lowest in energy for $I = 31$–39. The difference between experiment and calculations is shown in (c). Calculated noncollective aligned states are encircled.

peaks from the stronger ^{157,158}Er channels, which may have precluded the observation of the terminating 39^- state.

There are also predicted second aligned $I^\pi = 38^-, 39^-$ states that are formed in [5, 2] configurations with one antialigned $m_i = -11/2\, h_{11/2}$ proton, namely $\pi\{(d_{5/2}g_{7/2})^{-1}_{3/2,5/2}(h_{11/2})^5_{21/2}\}_{12,13^-} \otimes \nu\{(h_{9/2}f_{7/2})^4_{14}(i_{13/2})^2_{12}\}_{26^+}$ configurations. The $I^\pi = 38^-$ state, shown in Fig. 13(b), is calculated to be only ~300 keV above the fully aligned $I^\pi = 38^-$ [4, 1] state, but by considering uncertainties in the calculations it is not so evident which configuration should be assigned to the observed low-lying $I^\pi = 38^-$ state. A particularly low lying $I^\pi = 33^-$ state is observed in band 6a [see Fig. 3]. In the [4, 1] configuration, a low-lying oblate $I^\pi = 33^-$ state is calculated with one antialigned $h_{9/2}/f_{7/2}$ neutron, which may be naturally associated with the observed $I^\pi = 33^-$ state. Moreover, the fact that no corresponding low-lying $I^\pi = 33^-$ state is calculated in [5, 2] configurations suggests that the observed states for $I > 30$ should be associated with [4, 1] configurations.

The difficulty in observing very high spin states of negative parity might be caused by the large number of low-lying bands, as suggested from the calculated states of signature $\alpha = 0$ shown in Fig. 13(b). In a similar way, several bands at low energy are calculated for odd spins, $\alpha = 1$. For somewhat higher spins, a favored termination is calculated at $I^\pi = 46^-$ for the [5, 2] configuration [see Fig. 13(b)]. The highest spin range of this band has energies very close to those of the

$[4d_{3/2}, 2]$ band terminating at $I^\pi = 46^+$ in Fig. 12. This is understood from the fact that the difference between these two bands is that the fifth valence proton is either in the fifth $h_{11/2}$ orbital or in the lowest $d_{3/2}$ orbital, both with $m_i = 3/2$. As seen in Fig. 11(a), these two $m_i = 3/2\, h_{11/2}$ and $d_{3/2}$ orbitals come very close in energy, at the appropriate oblate deformation, yielding almost degenerate proton configurations with $I^\pi = 20^\pm$, which may be coupled to the $I^\pi = 26^+$ neutron configuration of Fig. 11(b). Therefore, if both positive- and negative-parity states of ^{156}Er could be observed up to $I = 46$, it would be very helpful to fix the position of the proton subshells around $Z = 64$ in more detail.

Only one state with $I = 43$ is shown in Fig. 3; it feeds the aligned $I^\pi = 42^+$ state of band 3 through the 1057-keV dipole transition. The favored candidate for this state is formed as the maximum-spin state in the [4, 3] configuration with $I^\pi = 43^-$, calculated to be approximately 1.4 MeV above the $I^\pi = 42^+$ aligned state. Another $I^\pi = 43^-$ state is calculated to be approximately 200 keV higher in energy in a [5, 2] configuration with $I_{\max} = 45$; these two states belong to signature partners of the [4, 3] and [5, 2] configurations, which terminate at $I = 44$ and 46, respectively, in Fig. 13(b). If, however, the $I = 43$ feeding state has positive parity, the most likely configuration would be the signature partner of the $[4d_{3/2}, 2]$ band drawn in Fig. 12. For this configuration, with $I_{\max} = 45$, the $I^\pi = 43^+$ state is calculated to lie approximately 1.65 MeV above the aligned $I^\pi = 42^+$ state of band 3.

5. *Systematics of N = 88 isotones at high spin*

The energies of $(\pi, \alpha) = (+, 0)$ bands in the $N = 88$ isotones ^{152}Gd [36], ^{154}Dy [37], and ^{158}Yb [5,38,39] are plotted, relative to a rotating liquid-drop reference, in Fig. 14, together with the results for ^{156}Er. The same reference is used for ^{156}Er as in other diagrams in this paper. For the other nuclei, the rotating liquid-drop energy, which is subtracted, is defined consistently for each specific nucleus [52]. Such plots comparing rotational bands in neighboring nuclei, but using less consistent parameters, were previously considered in Refs. [9,60]. It is informative to note the common features of the bands in Fig. 14. Because no average pairing energy is included in the reference, the ground-state energy is below zero for all the nuclei. It is then rather expensive to build angular momentum for spin values $I \approx 20$–30, as seen from the positive energy values around 1 MeV.

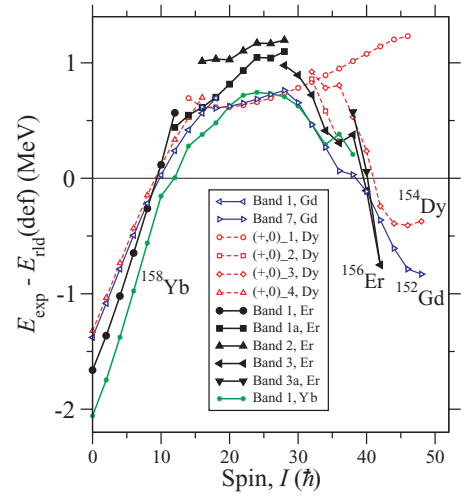

FIG. 14. (Color online) Energies of positive-parity, even-spin bands in several $N = 88$ isotones shown relative to a rotating liquid-drop reference. Except for ^{156}Er, only selective states are drawn (i.e., the yrast states for ^{152}Gd and ^{158}Yb), whereas coexisting high-spin bands, which are only observed in ^{154}Dy, are also shown for that nucleus.

At higher spin values, there are rotational bands in all nuclei that start to slope downward at $I \approx 30$, leading to terminations that are observed or predicted for spin values $I = 42$–52. The predicted band-terminating states are listed in Table VI for the nuclei shown in Fig. 14 and in addition for one more isotone, ^{160}Hf. The configurations are given relative to the $^{146}_{64}$Gd$_{82}$ doubly magic core, and also relative to the favored [4, 2] configuration of ^{156}Er. The neutron configuration, distributing six particles across $\nu i_{13/2}$ (2) and $\nu h_{9/2}/f_{7/2}$ (4) states, is rather stable and generates a spin of 26^+ for oblate shape. The $N = 88$ isotones then generate differing amounts of spin owing to the proton configurations. In ^{154}Dy, it is the $\pi(h_{11/2})^2_{10^+}$ configuration that builds the low-lying 36^+ state observed in this nucleus [37]. It appears that the $\pi(h_{11/2})^4_{16^+}$ configuration is also rather stable; this represents the proton valence configuration of $^{156}_{68}$Er. Lighter isotones can achieve this favored proton configuration through particle-hole excitations across the spherical $Z = 64$ shell gap (i.e., four-particle–four-hole excitations for ^{152}Gd and two-particle–two-hole excitations for ^{154}Dy), as shown in Table VI. The extra number of "valence" nucleons afforded by

TABLE VI. Predicted $(\pi, \alpha) = (+, 0)$ band-terminating states in $N = 88$ isotones, given relative to the $^{146}_{64}$Gd$_{82}$ core.

Nuclide	I^π	Aligned configuration	Configuration relative to ^{156}Er
^{152}Gd	52^+	$\pi\{(d_{5/2}/g_{7/2})^{-4}_{10}(h_{11/2})^4_{16}\}_{26^+} \otimes \nu\{(i_{13/2})^2_{12}(f_{7/2})^2_6(h_{9/2})^2_8\}_{26^+}$	$\pi\{(d_{5/2}/g_{7/2})^{-4}_{10}\}_{10^+} \otimes [4, 2]$
^{154}Dy	48^+	$\pi\{(d_{5/2}/g_{7/2})^{-2}_6(h_{11/2})^4_{16}\}_{22^+} \otimes \nu\{(i_{13/2})^2_{12}(f_{7/2})^2_6(h_{9/2})^2_8\}_{26^+}$	$\pi\{(d_{5/2}/g_{7/2})^{-2}_6\}_{6^+} \otimes [4, 2]$
^{156}Er	42^+	$\pi\{(h_{11/2})^4_{16}\}_{16^+} \otimes \nu\{(i_{13/2})^2_{12}(f_{7/2})^2_6(h_{9/2})^2_8\}_{26^+}$	$[4, 2]$
^{158}Yb	44^+	$\pi\{(d_{3/2})^2_2(h_{11/2})^4_{16}\}_{18^+} \otimes \nu\{(i_{13/2})^2_{12}(f_{7/2})^2_6(h_{9/2})^2_8\}_{26^+}$	$\pi\{(d_{3/2})^2_2\}_{2^+} \otimes [4, 2]$
^{158}Yb	44^+	$\pi\{(h_{11/2})^6_{18}\}_{18^+} \otimes \nu\{(i_{13/2})^2_{12}(f_{7/2})^2_6(h_{9/2})^2_8\}_{26^+}$	$\pi\{(h_{11/2})^2_2\}_{2^+} \otimes [4, 2]$
^{160}Hf	46^+	$\pi\{(d_{3/2})^2_2(h_{11/2})^6_{18}\}_{20^+} \otimes \nu\{(i_{13/2})^2_{12}(f_{7/2})^2_6(h_{9/2})^2_8\}_{26^+}$	$\pi\{(d_{3/2})^2_2(h_{11/2})^2_2\}_{4^+} \otimes [4, 2]$

these particle-hole excitatations can then generate spin beyond $I = 42$ (^{156}Er) such that terminating states are expected in ^{154}Dy and ^{152}Gd at $I = 48$ and 52, respectively. In contrast to the abrupt (favored) termination in ^{156}Er, the terminations in ^{154}Dy and ^{152}Gd appear smooth (unfavored) in nature (see Fig. 14); ^{154}Dy achieves termination at $I = 48$, whereas ^{152}Gd is also observed to $I = 48$, but is four units of spin off termination. For the heavier $N = 88$ isotones, the extra protons occupy further $\pi h_{11/2}$ states or $\pi d_{3/2}$ states [see Fig. 11(a)]. However, these states only provide low-spin projections (m_i), such that terminating states are expected in ^{158}Yb and ^{160}Hf at $I = 44$ and 46, respectively.

Another feature of Fig. 14 is the coexisting collective band in ^{154}Dy, labeled $(+, 0)\_1$, which has been observed up to $I = 46$; a similar negative-parity band (not shown in Fig. 14) has also been identified in ^{154}Dy up to $I^\pi = 51^-$ [37]. Analogous bands, based on the $\pi(h_{11/2})^6$ configuration, are also expected in the neighboring isotones, for example the calculated [6, 2] band of ^{156}Er included in Fig. 12. The ^{154}Dy bands are interpreted as having two $h_{11/2}$ holes in the $N = 82$ core. The corresponding [6, (02)2] band in ^{156}Er is however calculated to be somewhat higher in energy (see Fig. 12). In the case of ^{154}Dy ($Z = 66$), a favored $\pi\{(h_{11/2})^6(d_{5/2}/g_{7/2})^{-4}\}$ proton configuration is formed in a large region of deformation space. This is consistent with the fact that, up to now, ^{154}Dy is the only nucleus where such configurations have been observed. In addition, it is only in ^{154}Dy that detailed lifetime measurements have been made [61]. It would be valuable to perform similar lifetime measurements in other $N = 88$ nuclei.

IV. CONCLUSIONS

A high-statistics, high-spin experiment has been performed to study the level structure of the $^{156-158}$Er nuclei. Although not the dominant product, many new γ-ray transitions have been established in ^{156}Er and a comprehensive level scheme has been built from a high-fold analysis. The observation of many weak intraband transitions has allowed an investigation of $B(M1)/B(E2)$ and $B(E1)/B(E2)$ ratios, and consequently $B(M1)$ and $B(E1)$ strengths have been deduced. Relatively large $B(E1)$ strengths of 10^{-3} W.u., in addition to low-lying negative-parity states (yrast for $I \sim 10$), may suggest a role for octupole collectivity in this nucleus at low spin, similar to lighter $N = 88$ isotones.

At higher spin, the structure of ^{156}Er evolves towards a weakly deformed oblate-triaxial shape and band-terminating states have been confirmed at $I^\pi = 42^+$ and $I^\pi = 38^-$. Five weak transitions of energies in the range 1.0–2.2 MeV have been observed feeding the energetically favored $I^\pi = 42^+$ terminating state, with four of them newly identified in this work. Four of these transitions have angular distributions consistent with quadrupole ($E2$) nature, whereas the fifth transition appears to be a $\Delta I = 1$ dipole transition. Cranked Nilsson-Strutinsky calculations indicate that the feeding transitions originate from configurations involving a core-breaking proton particle-hole excitation, namely $\pi d_{5/2}/g_{7/2} \rightarrow d_{3/2}$, across the semi-magic $Z = 64$ shell gap.

The systematics of the $N = 88$ isotones have been examined at high spin for $Z = 64$ to 70. These results now form a compelling body of data displaying remarkably similar general evolutionary features, along with particularly favored nuclear states corresponding to specific configurations, providing strong evidence for a transition from prolate collective rotation to oblate noncollective excitations via the mechanism of band termination. This process represents a beautiful manifestation of mesoscopic physics since the underlying finite-particle basis of nuclear angular momentum generation is revealed.

ACKNOWLEDGMENTS

We are indebted to Dr. D. C. Radford for providing the RadWare analysis codes and to the accelerator staff at the Lawrence Berkeley National Laboratory. This work was supported in part by the United Kingdom Engineering and Physical Sciences Research Council (EPSRC) and Science and Technology Facilities Council (STFC), the U.S. Department of Energy under Contract No. AC03-76SF00098, the National Science Foundation, the State of Florida, and the Swedish Science Research Council.

[1] A. Bohr and B. R. Mottelson, Phys. Scr. A **10**, 13 (1974).
[2] J. Pedersen *et al.*, Phys. Rev. Lett. **39**, 990 (1977).
[3] T. Bengtsson and I. Ragnarsson, Phys. Scr. **T5**, 165 (1983).
[4] I. Ragnarsson, V. P. Janzen, D. B. Fossan, N. C. Schmeing, and R. Wadsworth, Phys. Rev. Lett. **74**, 3935 (1995).
[5] C. Baktash *et al.*, Phys. Rev. Lett. **54**, 978 (1985).
[6] I. Ragnarsson, T. Bengtsson, W. Nazarewicz, J. Dudek, and G. A. Leander, Phys. Rev. Lett. **54**, 982 (1985).
[7] F. S. Stephens, M. A. Deleplanque, R. M. Diamond, A. O. Macchiavelli, and J. E. Draper, Phys. Rev. Lett. **54**, 2584 (1985).
[8] I. Ragnarsson and T. Bengtsson, Nucl. Phys. **A447**, 251 (1985).
[9] I. Ragnarsson, Z. Xing, T. Bengtsson, and M. A. Riley, Phys. Scr. **34**, 651 (1986).
[10] J. Dudek and W. Nazarewicz, Phys. Rev. C **31**, 298 (1985).
[11] A. V. Afanasjev, D. B. Fossan, G. J. Lane, and I. Ragnarsson, Phys. Rep. **322**, 1 (1999).
[12] N. Nica *et al.*, Phys. Rev. C **64**, 034313 (2001).
[13] S. J. Gale *et al.*, J. Phys. G **21**, 193 (1995).
[14] J. Simpson *et al.*, Phys. Lett. **B327**, 187 (1994).
[15] A. O. Evans *et al.*, Phys. Rev. Lett. **92**, 252502 (2004).
[16] A. O. Evans *et al.*, Phys. Rev. C **73**, 064303 (2006).
[17] K. Heyde, *Basic Ideas and Concepts in Nuclear Physics* (Institute of Physics, London, 1999), p. 53.
[18] S. G. Nilsson and I. Ragnarsson, *Shapes and Shells in Nuclear Structure* (Cambridge University Press, Cambridge, 1995), p. 230.
[19] M. A. Riley *et al.*, Phys. Scr. T **125**, 123 (2006).
[20] A. Pipidis, Ph.D. thesis, Florida State University, 2006.
[21] F. Azgui *et al.*, Z. Phys. A **320**, 699 (1985).
[22] I. Y. Lee, Nucl. Phys. **A520**, 641c (1990).
[23] D. C. Radford, Nucl. Instrum. Methods Phys. Res. A **361**, 297 (1995).
[24] D. C. Radford, M. Cromaz, and C. J. Beyer, in *Proceedings of the Nuclear Structure '98 Conference, Gatlinburg, 1998*, edited by

C. Baktash (American Institute of Physics, College Park, MD, 1999), p. 570.
[25] C. W. Beausang *et al.*, Nucl. Instrum. Methods Phys. Res. A **364**, 560 (1995).
[26] E. S. Paul *et al.*, Phys. Rev. Lett. **98**, 012501 (2007).
[27] H. Beuscher, W. F. Davidson, R. M. Lieder, and C. Mayer-Böricke, Z. Phys. **263**, 201 (1973).
[28] C. W. Reich, Nucl. Data Sheets **99**, 753 (2003), and references therein.
[29] J. Jolie, R. F. Casten, P. Cejnar, S. Heinze, E. A. McCutchan, and N. V. Zamfir, Phys. Rev. Lett. **93**, 132501 (2004).
[30] J. A. Sheikh, G. H. Bhat, Y. Sun, G. B. Vakil, and R. Palit, Phys. Rev. C **77**, 034313 (2008).
[31] T. Bengtsson, Nucl. Phys. **A512**, 124 (1990).
[32] R. Bengtsson and S. Frauendorf, Nucl. Phys. **A327**, 139 (1979).
[33] S. M. Harris, Phys. Rev. **138**, B509 (1965).
[34] J. Simpson *et al.*, J. Phys. G: Nucl. Phys. **12**, L67 (1986).
[35] M. Ploszajczak and A. Faessler, Z. Phys. A **283**, 349 (1977).
[36] D. B. Campbell *et al.*, Phys. Rev. C **75**, 064314 (2007).
[37] W. C. Ma *et al.*, Phys. Rev. C **65**, 034312 (2002).
[38] S. B. Patel, F. S. Stephens, J. C. Bacelar, E. M. Beck, M. A. Deleplanque, R. M. Diamond, and J. E. Draper, Phys. Rev. Lett. **57**, 62 (1986).
[39] T. D. Baldwin, M.Phys. thesis, University of Surrey, 2002.
[40] K. Y. Ding *et al.*, Phys. Rev. C **62**, 034316 (2000).
[41] D. T. Joss *et al.* (to be published).
[42] G. D. Dracoulis, B. Fabricius, P. M. Davidson, A. O. Macchiavelli, J. Oliviera, J. Burde, F. Stephens, and M. A. Deleplanque, in *Proceedings of the International Conference on Nuclear Structure at High Angular Momentum, Ottawa, 1992* (Atomic Energy of Canada, Limited, Ottawa, 1992), AECL-10613, Vol 2, p. 94.
[43] J. Simpson *et al.*, Eur. Phys. J. A **1**, 267 (1998).
[44] P. Möller, J. R. Nix, W. D. Myers, and W. J. Swiatecki, At. Data Nucl. Data Tables **59**, 185 (1995).
[45] A. Bohr and B. R. Mottelson, *Nuclear Structure* (Benjamin, New York, 1975), Vol. II.
[46] P. A. Butler and W. Nazarewicz, Nucl. Phys. **A533**, 249 (1991).
[47] W. Nazarewicz and S. L. Tabor, Phys. Rev. C **45**, 2226 (1992).
[48] W. Nazarewicz, J. Dudek, R. Bengtsson, T. Bengtsson, and I. Ragnarsson, Nucl. Phys. **A435**, 397 (1985).
[49] S. Cwiok, J. Dudek, W. Nazarewicz, W. Skalski, and T. Werner, Comput. Phys. Commun. **46**, 379 (1987).
[50] J. Skalski, Phys. Rev. C **43**, 140 (1991).
[51] T. Bengtsson and I. Ragnarsson, Nucl. Phys. **A436**, 14 (1985).
[52] B. G. Carlsson and I. Ragnarsson, Phys. Rev. C **74**, 011302(R) (2006).
[53] K. Pomorski and J. Dudek, Phys. Rev. C **67**, 044316 (2003).
[54] K. T. R. Davies and J. R. Nix, Phys. Rev. C **14**, 1977 (1976).
[55] G. Andersson, S. E. Larsson, G. Leander, P. Moller, S. G. Nilsson, I. Ragnarsson, S. Aberg, R. Bengtsson, J. Dudek, B. Nerlo-Pomorska, K. Pomorski, and Z. Szymanski, Nucl. Phys. **A268**, 205 (1976).
[56] M. Zalewski, W. Satula, W. Nazarewicz, G. Stoitcheva, and H. Zduńczuk, Phys. Rev. C **75**, 054306 (2007).
[57] M. A. Riley *et al.*, Acta Phys. Pol. **40**, 513 (2009).
[58] K. Lagergren *et al.*, Phys. Rev. Lett. **87**, 022502 (2001).
[59] J. Ollier *et al.* (submitted to Phys. Rev. C).
[60] I. Ragnarsson, F. G. Kondev, E. S. Paul, M. A. Riley, and J. Simpson, Int. J. Mod. Phys. E **13**, 87 (2004).
[61] W. C. Ma *et al.*, Phys. Rev. Lett. **61**, 46 (1988).